Black-hole solutions with scalar hair in Einstein-scalar-Gauss-Bonnet theories

G. Antoniou,[1,2,*] A. Bakopoulos,[2,†] and P. Kanti[2,‡]

[1]School of Physics and Astronomy, University of Minnesota, Minneapolis, Minnesota 55455, USA
[2]Division of Theoretical Physics, Department of Physics, University of Ioannina, Ioannina GR-45110, Greece

(Received 21 November 2017; published 23 April 2018)

In the context of the Einstein-scalar-Gauss-Bonnet theory, with a general coupling function between the scalar field and the quadratic Gauss-Bonnet term, we investigate the existence of regular black-hole solutions with scalar hair. Based on a previous theoretical analysis, which studied the evasion of the old and novel no-hair theorems, we consider a variety of forms for the coupling function (exponential, even and odd polynomial, inverse polynomial, and logarithmic) that, in conjunction with the profile of the scalar field, satisfy a basic constraint. Our numerical analysis then always leads to families of regular, asymptotically flat black-hole solutions with nontrivial scalar hair. The solution for the scalar field and the profile of the corresponding energy-momentum tensor, depending on the value of the coupling constant, may exhibit a nonmonotonic behavior, an unusual feature that highlights the limitations of the existing no-hair theorems. We also determine and study in detail the scalar charge, horizon area, and entropy of our solutions.

DOI: 10.1103/PhysRevD.97.084037

I. INTRODUCTION

The construction of generalized gravitational theories, with the inclusion of extra fields or higher-curvature terms in the action, has attracted an enormous interest during the last decades [1,2]. The main reason is that these theories may provide the framework for the ultimate theory of gravity in the context of which several problems of the traditional General Relativity may be resolved. Therefore, in the context of these modified gravitational theories, different aspects of gravity, from black-hole solutions to cosmological solutions, have been readdressed and, on several occasions, shown to lead to novel, interesting solutions.

Such a class of solutions was the one describing regular black holes with a nontrivial scalar field in the exterior region, a type of solutions forbidden by General Relativity. In an attempt to construct a criterion of which the fulfillment or violation could, respectively, forbid or allow the emergence of such solutions, no-hair theorems were formed. In its first form, the *old no-hair theorem* [3] excluded static black holes with a scalar field; however, this was soon outdated by the discovery of black holes with Yang-Mills [4], Skyrme fields [5], or a conformal coupling to gravity [6]. These led to the formulation of the *novel no-hair theorem* [7] that was recently extended to cover the case of standard scalar-tensor theories [8]; a new form that covers the case of Galileon fields was also proposed [9].

However, in a limited number of theories, even the novel no-hair theorem may be evaded. The first counterexample appeared very soon after its formulation and demonstrated the existence of regular black holes with a scalar hair in the context of the Einstein-dilaton-Gauss-Bonnet theory [10] (for some earlier studies that paved the way, see Refs. [11–15]). Additional solutions in the context of the same theory were derived in the presence of a Yang-Mills field [16,17], in an arbitrary number of dimensions [18], or in the case of rotation [19–22] (for a number of interesting reviews on the topic, see Refs. [23–25]). The more recent form of the novel no-hair theorem [9] was also shown to be evaded [26], and concrete solutions were constructed [27,28].

A common feature of the theories that evaded the no-hair theorems was the presence of higher-curvature terms, such as the quadratic Gauss-Bonnet (GB) term inspired by the string theory [29] or Horndeski theory [30]. It is the presence of such terms that invalidate basic requirements of the no-hair theorems and open the way for the construction of black-hole solutions with scalar hair. In a recent work of ours [31], we considered a general class of Einstein-scalar-GB theories, of which the cases [10,26] constitute particular examples. We demonstrated that, under certain constraints on the form of the coupling

*anton296@umn.edu
†abakop@cc.uoi.gr
‡pkanti@cc.uoi.gr

function between the scalar field and the Gauss-Bonnet term, and in conjunction with the profile of the scalar field itself, a regular black-hole horizon regime and an asymptotically flat regime may be smoothly connected, and thus the no-hair theorems may be evaded. A number of novel black-hole solutions with scalar hair was thus determined and briefly presented [31].

In the present work, we provide additional support to the arguments presented in Ref. [31]. We consider a general gravitational theory containing the Ricci scalar, a scalar field, and the GB term, with the latter two quantities being coupled together through a coupling function $f(\phi)$. Guided by the findings of our previous work [31], we impose the aforementioned constraints on the coupling function f and the scalar field ϕ and investigate the existence of regular, black-hole solutions with a nontrivial scalar hair. We find a large number of such solutions for a variety of forms for the coupling function: exponential, polynomial (even and odd), inverse polynomial (even and odd), and logarithmic. In all cases, the solutions for the metric components, scalar field, curvature-invariant quantities, and components of the energy-momentum tensor are derived and discussed. Further characteristics of the produced solutions, such as the scalar charge, horizon area, and entropy, are also determined, studied in detail, and compared to the corresponding Schwarzschild values.

II. THEORETICAL FRAMEWORK

We start with the following action functional that describes a general class of higher-curvature gravitational theories [31]:

$$S=\frac{1}{16\pi}\int d^4x\sqrt{-g}\left[R-\frac{1}{2}\partial_\mu\phi\partial^\mu\phi+f(\phi)R^2_{\rm GB}\right]. \quad (1)$$

In this, the Einstein-Hilbert term given by the Ricci scalar curvature R is accompanied by the quadratic GB term $R^2_{\rm GB}$ defined as

$$R^2_{\rm GB}=R_{\mu\nu\rho\sigma}R^{\mu\nu\rho\sigma}-4R_{\mu\nu}R^{\mu\nu}+R^2, \quad (2)$$

in terms of the Riemann tensor $R_{\mu\nu\rho\sigma}$, Ricci tensor $R_{\mu\nu}$, and the Ricci scalar R. A scalar field ϕ also appears in the action (1) and couples to the GB term through a general coupling function $f(\phi)$. This is a necessary requirement in order for the GB term, which is a total derivative in four dimensions, to contribute to the field equations.

The gravitational field equations and the equation for the scalar field may be derived by varying the action (1) with respect to the metric tensor $g_{\mu\nu}$ and the scalar field ϕ, respectively. These have the form

$$G_{\mu\nu}=T_{\mu\nu}, \quad (3)$$

$$\nabla^2\phi+\dot{f}(\phi)R^2_{\rm GB}=0, \quad (4)$$

where $G_{\mu\nu}$ is the Einstein tensor and $T_{\mu\nu}$ is the energy-momentum tensor. The latter receives contributions from both the scalar field and the Gauss-Bonnet term and is given by

$$T_{\mu\nu}=-\frac{1}{4}g_{\mu\nu}\partial_\rho\phi\partial^\rho\phi+\frac{1}{2}\partial_\mu\phi\partial_\nu\phi -\frac{1}{2}(g_{\rho\mu}g_{\lambda\nu}+g_{\lambda\mu}g_{\rho\nu})\eta^{\kappa\lambda\alpha\beta}\tilde{R}^{\rho\gamma}{}_{\alpha\beta}\nabla_\gamma\partial_\kappa f(\phi), \quad (5)$$

with

$$\tilde{R}^{\rho\gamma}{}_{\alpha\beta}=\eta^{\rho\gamma\sigma\tau}R_{\sigma\tau\alpha\beta}=\frac{\epsilon^{\rho\gamma\sigma\tau}}{\sqrt{-g}}R_{\sigma\tau\alpha\beta}. \quad (6)$$

Throughout this work, the dot over the coupling function denotes its derivative with respect to the scalar field (i.e., $\dot{f}=df/d\phi$), and we employ units in which $G=c=1$.

Our aim is to find solutions of the set of Eqs. (3) and (4) that describe regular, static, asymptotically flat black-hole solutions with a nontrivial scalar field. In particular, we will assume that the line element takes the spherically symmetric form

$$ds^2=-e^{A(r)}dt^2+e^{B(r)}dr^2+r^2(d\theta^2+\sin^2\theta d\varphi^2) \quad (7)$$

and that the scalar field is also static and spherically symmetric, $\phi=\phi(r)$. In our quest for the aforementioned solutions, we will consider a variety of coupling functions $f(\phi)$, which will, however, need to obey certain constraints [31].

By employing the line element (7), we may obtain the explicit forms of Eqs. (3) and (4): the (tt), (rr), and $(\theta\theta)$ components of Einstein's equations then, respectively, read

$$4e^B(e^B+rB'-1) =\phi'^2[r^2e^B+16\ddot{f}(e^B-1)] -8\dot{f}[B'\phi'(e^B-3)-2\phi''(e^B-1)], \quad (8)$$

$$4e^B(e^B-rA'-1)=-\phi'^2r^2e^B+8(e^B-3)\dot{f}A'\phi', \quad (9)$$

$$e^B[rA'^2-2B'+A'(2-rB')+2rA''] =-\phi'^2(re^B-8\ddot{f}A') +4\dot{f}[A'^2\phi'+2\phi'A''+A'(2\phi''-3B'\phi')], \quad (10)$$

while the equation for the scalar field takes the form

$$2r\phi''+(4+rA'-rB')\phi'+\frac{4\dot{f}e^{-B}}{r}[(e^B-3)A'B' -(e^B-1)(2A''+A'^2)]=0. \quad (11)$$

In the above, the prime in the metric functions A and B and the scalar field ϕ denote their differentiation with respect to the radial coordinate r.

Before being able to numerically integrate the system of Eqs. (8)–(11), we need to reduce the number of independent variables. We observe that the (rr) component (9) may take the form of a second-order polynomial with respect to e^B, i.e., $e^{2B}+\beta e^B+\gamma=0$. Therefore, this can be solved to give

$$e^B=\frac{-\beta\pm\sqrt{\beta^2-4\gamma}}{2}, \tag{12}$$

where

$$\beta=\frac{r^2\phi'^2}{4}-(2\dot{f}\phi'+r)A'-1, \qquad \gamma=6\dot{f}\phi'A'. \tag{13}$$

According to the above, the solution for the metric function $B(r)$ may be easily found once the solutions for the scalar field $\phi(r)$ and the metric function $A(r)$ are determined. In the remaining system of Eqs. (8), (10), and (11), e^B may therefore be eliminated by using Eq. (12), while B' may be replaced by the expression

$$B'=-\frac{\gamma'+\beta' e^B}{2e^{2B}+\beta e^B}, \tag{14}$$

which follows by differentiating Eq. (12) with respect to the radial coordinate. Subsequently, the remaining three equations (8), (10), and (11) form a system of only two independent, ordinary differential equations of second order for the functions A and ϕ:

$$A''=\frac{P}{S}, \tag{15}$$

$$\phi''=\frac{Q}{S}. \tag{16}$$

In the above equations, P, Q, and S are complicated expressions of $(r, e^B, \phi', A', \dot{f}, \ddot{f})$ that are given in the Appendix. Note that in these expressions we have eliminated, via Eq. (14), B' that involves A'' and ϕ'' but retained e^B for notational simplicity.

A. Asymptotic solution at black-hole horizon

We will start our quest for black-hole solutions with a nontrivial scalar hair by determining first the asymptotic solutions of the set of Eqs. (8)–(11) near the black-hole horizon and at asymptotic infinity. These solutions will serve as boundary conditions for our numerical integration but will also provide important constraints on our theory (1). Near the black-hole horizon r_h, it is usually assumed that the metric functions and the scalar field may be expanded as

$$e^A=\sum_{n=1}^{\infty}a_n(r-r_h)^n, \tag{17}$$

$$e^{-B}=\sum_{n=1}^{\infty}b_n(r-r_h)^n, \tag{18}$$

$$\phi=\sum_{n=0}^{\infty}\frac{\phi^{(n)}(r_h)}{n!}(r-r_h)^n, \tag{19}$$

where (a_n, b_n) are constant coefficients and $\phi^{(n)}(r_h)$ denotes the (nth) derivative of the scalar field evaluated at the black-hole horizon. Equations (17) and (18) reflect the expected behavior of the metric tensor near the horizon of a spherically symmetric black hole with the solution being regular if the scalar coefficients $\phi^{(n)}(r_h)$ in Eq. (19) remain finite at the same regime.

In a recent work of ours [31], we followed instead the alternative approach of assuming merely that, near the horizon, the metric function $A(r)$ diverges, in accordance with Eq. (17). Then, the system of differential equations was evaluated in the limit $r\to r_h$, and the finiteness of the quantity ϕ'' was demanded. This approach was followed in Ref. [10], in which an exponential coupling function was assumed between the scalar field and the GB term. In Ref. [31], the form of the coupling function $f(\phi)$ was left arbitrary, and the requirement of the finiteness of ϕ_h'' was shown to be satisfied only under the constraint

$$r_h^3\phi_h'+12\dot{f}_h+2r_h^2\phi_h'^2\dot{f}_h=0, \tag{20}$$

where all quantities have been evaluated at the horizon r_h. The above is a second-order polynomial with respect to ϕ_h' and may be easily solved to yield the solutions

$$\phi_h'=\frac{r_h}{4\dot{f}_h}\left(-1\pm\sqrt{1-\frac{96\dot{f}_h^2}{r_h^4}}\right). \tag{21}$$

The above ensures that an asymptotic black-hole solution with a regular scalar field exists for a general class of theories of the form (1). The only constraint on the form of the coupling function arises from the demand that the first derivative of the scalar field on the horizon must be real, which translates to the inequality

$$\dot{f}_h^2<\frac{r_h^4}{96}. \tag{22}$$

Assuming the validity of the constraint (20), Eq. (15) then uniquely determines the form of the metric function A in the near-horizon regime; through Eq. (12), the metric function B is also determined. Therefore, the asymptotic solution of Eqs. (12), (15), and (16), in the limit $r\to r_h$, is given by the expressions

$$e^{A} = a_1(r - r_h) + \cdots, \tag{23}$$

$$e^{-B} = b_1(r - r_h) + \cdots, \tag{24}$$

$$\phi = \phi_h + \phi_h'(r - r_h) + \phi_h''(r - r_h)^2 + \cdots \tag{25}$$

and describes, by construction, a black-hole horizon with a regular scalar field provided that ϕ' obeys the constraint (21) and the coupling function f satisfies Eq. (22). We note that the desired form of the asymptotic solution was derived only for the choice of the (+) sign in Eq. (12) as the (−) sign fails to lead to a black-hole solution [31].

The aforementioned regularity of the near-horizon solution should be reflected to the components of the energy-momentum tensor $T_{\mu\nu}$ as well as to the scalar invariant quantities of the theory. The nonvanishing components of the energy-momentum tensor (5) are

$$T^{t}{}_{t} = -\frac{e^{-2B}}{4r^2}[\phi'^2(r^2e^B + 16\ddot{f}(e^B - 1)) - 8\dot{f}(B'\phi'(e^B - 3) - 2\phi''(e^B - 1))], \tag{26}$$

$$T^{r}{}_{r} = \frac{e^{-B}\phi'}{4}\left[\phi' - \frac{8e^{-B}(e^B - 3)\dot{f}A'}{r^2}\right], \tag{27}$$

$$T^{\theta}{}_{\theta} = T^{\varphi}{}_{\varphi} = -\frac{e^{-2B}}{4r}[\phi'^2(re^B - 8\ddot{f}A') - 4\dot{f}(A'^2\phi' + 2\phi'A'' + A'(2\phi'' - 3B'\phi'))]. \tag{28}$$

Employing the asymptotic behavior given in Eqs. (23)–(25), we readily derive the following approximate behavior:

$$T^{t}{}_{t} = +\frac{2e^{-B}}{r^2}B'\phi'\dot{f} + \mathcal{O}(r - r_h), \tag{29}$$

$$T^{r}{}_{r} = -\frac{2e^{-B}}{r^2}A'\phi'\dot{f} + \mathcal{O}(r - r_h), \tag{30}$$

$$T^{\theta}{}_{\theta} = T^{\varphi}{}_{\varphi} = \frac{e^{-2B}}{r}\phi'\dot{f}(2A'' + A'^2 - 3A'B') + \mathcal{O}(r - r_h). \tag{31}$$

The above expressions, in the limit $r \to r_h$, lead to constant values for all components of the energy-momentum tensor. Similarly, one may see that the scalar invariant quantities R, $R_{\mu\nu}R^{\mu\nu}$ and $R_{\mu\nu\rho\sigma}R^{\mu\nu\rho\sigma}$, the exact expressions of which are listed in the Appendix, reduce to the approximate forms

$$R = +\frac{2e^{-B}}{r^2}(e^B - 2rA') + \mathcal{O}(r - r_h), \tag{32}$$

$$R_{\mu\nu}R^{\mu\nu} = +\frac{2e^{-2B}}{r^4}(e^B - rA')^2 + \mathcal{O}(r - r_h), \tag{33}$$

$$R_{\mu\nu\rho\sigma}R^{\mu\nu\rho\sigma} = +\frac{4e^{-2B}}{r^4}(e^{2B} + r^2A'^2) + \mathcal{O}(r - r_h). \tag{34}$$

In the above, we have used that, near the horizon, $A' \approx -B' \approx 1/(r - r_h)$ and $A'^2 \approx -A''$, as dictated by Eqs. (23) and (24). Again, the dominant term in each curvature invariant adopts a constant, finite value in the limit $r \to r_h$. Subsequently, the GB term also turns out to be finite, in the same limit, and is given by

$$R^2_{\mathrm{GB}} = +\frac{12e^{-2B}}{r^4}A'^2 + \mathcal{O}(r - r_h). \tag{35}$$

B. Asymptotic solution at infinity

At the other asymptotic regime, that of radial infinity ($r \to \infty$), the metric functions, and the scalar field may be again expanded in power series, this time in terms of $1/r$. Demanding that the metric components reduce to those of the asymptotically flat Minkowski space-time while the scalar field assumes a constant value, we write

$$e^{A} = 1 + \sum_{n=1}^{\infty}\frac{p_n}{r}, \tag{36}$$

$$e^{B} = 1 + \sum_{n=1}^{\infty}\frac{q_n}{r}, \tag{37}$$

$$\phi = \phi_\infty + \sum_{n=1}^{\infty}\frac{d_n}{r}. \tag{38}$$

The arbitrary coefficients (p_n, q_n, d_n) are in principle determined upon substitution of Eqs. (36)–(38) in the field equations of the theory. However, two of the coefficients, namely, p_1 and d_1, remain as free parameters and are associated with the Arnowitt-Deser-Misner mass and scalar charge, respectively: $p_1 \equiv -2M$ and $d_1 = D$. The remaining coefficients may be calculated to an arbitrary order: we have performed this calculation up to order $\mathcal{O}(1/r^6)$ and derived the following expressions:

$$e^{A} = 1 - \frac{2M}{r} + \frac{MD^2}{12r^3} + \frac{24MD\dot{f} + M^2D^2}{6r^4} - \frac{96M^3D - 3MD^3 + 512M^2\dot{f} - 64D^2\dot{f} + 128MD^2\ddot{f}}{90r^5} + \mathcal{O}(1/r^6), \tag{39}$$

$$e^B = 1 + \frac{2M}{r} + \frac{16M^2 - D^2}{4r^2} + \frac{32M^3 - 5MD^2}{4r^3} + \frac{768M^4 - 208M^2D^2 - 384MD\dot{f} + 3D^4}{48r^4} + \frac{6144M^5 - 2464M^3D^2 + 97MD^4 - 6144M^2D\dot{f} + 192D^3\dot{f} - 384MD^2\ddot{f}}{192r^5} + \mathcal{O}(1/r^6), \tag{40}$$

$$\phi = \phi_\infty + \frac{D}{r} + \frac{MD}{r^2} + \frac{32M^2D - D^3}{24r^3} + \frac{12M^3D - 24M^2\dot{f} - MD^3}{6r^4} + \frac{6144M^4D - 928M^2D^3 + 9D^5 - 12288M^3\dot{f} - 1536MD^2\dot{f}}{1920r^5} + \mathcal{O}(1/r^6). \tag{41}$$

We observe that the scalar charge D modifies significantly the expansion of the metric functions at order $\mathcal{O}(1/r^2)$ and higher. The existence itself of D, and thus of a nontrivial form for the scalar field, is caused by the presence of the GB term in the theory. The exact form, however, of the coupling function does not enter in the above expansions earlier than the order $\mathcal{O}(1/r^4)$. This shows that an asymptotically flat solution of Eqs. (8)–(11), with a constant scalar field does not require a specific coupling function and, in fact, arises for an arbitrary form of this function.

The asymptotic solution at infinity, given by Eqs. (36)–(38), is also characterized by regular components of $T_{\mu\nu}$ and curvature invariants. Employing the facts that, as $r \to \infty$, $(e^A, e^B, \phi) \approx \mathcal{O}(1)$ while $(A', B', \phi') \approx \mathcal{O}(1/r^2)$, we find for the components of the energy-momentum tensor the asymptotic behavior

$$T^t{}_t \simeq -T^r{}_r \simeq T^\theta{}_\theta \simeq -\frac{1}{4}\phi'^2 + \mathcal{O}\left(\frac{1}{r^6}\right). \tag{42}$$

Clearly, all of the above components go to zero, as expected. Similar behavior is exhibited by all curvature invariants and the GB term, in accordance with the asymptotically flat limit derived above. In particular, for the GB term, we obtain

$$R^2_{\rm GB} \approx \frac{48M^2}{r^6}. \tag{43}$$

C. Connecting the two asymptotic solutions

In the previous two subsections, we have constructed a near-horizon solution with a regular scalar field and an asymptotically flat solution with a constant scalar field—which was achieved under mild constraints on the form of the coupling function $f(\phi)$. However, given the complexity of the equations of the theory, it is the numerical integration of the system (15) and (16) that will reveal whether these two asymptotic solutions may be smoothly matched to create a black-hole solution with scalar hair valid over the entire radial domain.

In fact, theoretical arguments developed decades ago, the so-called no-hair theorems, excluded in the past the emergence of such solutions in a variety of scalar-tensor theories. The older version of the no-hair theorem [3] was applied in theories with minimally coupled scalar fields: it employs the scalar equation of motion and relies on the sign of $V'(\phi)$, where $V(\phi)$ is the potential of the scalar field. In most theories studied, the quantity $V'(\phi)$ had the sign opposite of the demanded one, and this excluded the emergence of the desired black-hole solutions. In Ref. [31], the same argument was applied in the case of the theory (1), appropriately altered to yield a constraint on the effective potential $V_{\rm eff}(\phi) = f(\phi)R^2_{\rm GB}$ of the scalar field. Although this constraint was of an integral form over the entire radial regime, in special cases, it merely demanded that $f(\phi)R^2_{\rm GB} > 0$. In Eqs. (35) and (43), the asymptotic values of the GB term near the horizon and at infinity were derived: they are both positive, with the latter decreasing as r increases. These results point to a monotonic decreasing behavior of the GB term from an initial positive value near the horizon to a vanishing value at radial infinity—as we will shortly demonstrate in the next section, this is indeed the behavior of the GB term. In that case, the only requirement for the evasion of the old no-hair theorem is apparently the positivity of the coupling function $f(\phi)$.

As the old no-hair theorem imposes in general mild constraints on a theory, in Ref. [31], we considered in addition the novel no-hair theorem [7] that applies also in theories with a conformal coupling of the scalar fields to gravity (see also Ref. [8]). This argument relies on the profile of the $T^r{}_r$ component of the energy-momentum tensor of the theory in terms of the radial coordinate. In a large class of theories, under the assumptions of positivity and conservation of energy, it is in general extremely difficult to smoothly match the near-horizon and asymptotic-infinity values of $T^r{}_r$. That prevents the emergence of black-hole solutions with scalar hair. However, the novel no-hair theorem was shown to be evaded in the context of the Einstein-scalar-Gauss-Bonnet theory with an exponential coupling function [10] or a linear coupling function [26]. In both theories, the presence of the GB term played a catalytic role for the emergence of the solutions. Therefore, in Ref. [31], we kept again the form of the coupling function $f(\phi)$ arbitrary and reconsidered the argument of

the novel no-hair theorem. Our analysis revealed that the evasion of this theorem holds for a general class of theories involving the GB term: the profile of $T^r{}_r$ in terms of r may be easily made smooth and monotonic under the assumptions that, near the horizon,

$$\dot{f}\phi' < 0, \qquad \dot{f}\phi'' + \ddot{f}\phi'^2 > 0. \tag{44}$$

The first constraint, according to Eq. (30), ensures the positivity of $T^r{}_r$ in the near-horizon regime; the second ensures that $(T^r{}_r)'$ is negative in the same regime. Then, in conjunction with the behavior described by Eq. (42) at radial infinity, $T^r{}_r$ is positive and decreasing over the whole radial regime. This behavior invalidates the requirements set by the novel no-hair theorem and thus causes its evasion.

In fact, the first of the constraints listed in Eq. (44) is already satisfied: Eq. (21) dictates that the combination $\dot{f}\phi'$ at the horizon is always negative to ensure the regularity of the black-hole horizon. Therefore, if $\dot{f} > 0$, then ϕ'_h must be necessarily negative, or vice versa. The remaining constraint $\dot{f}\phi'' + \ddot{f}\phi'^2 > 0$ may be alternatively written as $\partial_r(\dot{f}\phi')|_{r_h} > 0$; this merely demands that the aforementioned negative value of the quantity $(\dot{f}\phi')|_{r_h}$ should be constrained away from the horizon so that the two asymptotic solutions (23)–(25) and (36)–(38) can smoothly match. As we will see in the next section, this second constraint is automatically satisfied for all the solutions found and does not demand any fine-tuning of our parameters.

III. NUMERICAL SOLUTIONS

The derivation of exact solutions, valid over the entire radial domain, demands the numerical integration of the system (15) and (16). Our integration starts at a distance very close to the horizon of the black hole, i.e., at $r \approx r_h + \mathcal{O}(10^{-5})$ (for simplicity, we set $r_h = 1$). There, we use as boundary conditions the asymptotic solution (23)–(25) together with Eq. (21) for ϕ'_h upon choosing a particular coupling function $f(\phi)$. The integration proceeds toward large values of the radial coordinate until the form of the derived solution matches the asymptotic solution (36)–(38). In the next subsections, we present a variety of regular black-hole solutions with scalar hair for different choices of the coupling function $f(\phi)$.

A. Exponential coupling function

First, we consider the case in which $f(\phi) = \alpha e^{\kappa\phi}$. According to the arguments presented in Sec. II .3, the evasion of the old no-hair theorem is ensured for $f(\phi) > 0$; therefore, we focus on the case with $\alpha > 0$. As the exponential function is always positive definite, the sign of $\dot{f} = \alpha\kappa e^{\kappa\phi}$ is then determined by the sign of κ. To evade also the novel no-hair theorem and allow for regular black-hole solutions to emerge, we should satisfy the constraint $\dot{f}\phi' < 0$, or equivalently $\kappa\phi' < 0$, near the horizon. Therefore, for $\kappa > 0$, we should have $\phi'_h < 0$, which causes the decreasing of the scalar field as we move away from the black-hole horizon. The situation is reversed for $\kappa < 0$ when ${\phi_h}' > 0$ and the scalar field increases with r.

The case of $f(\phi) = \alpha e^{\phi}$, with $\alpha > 0$, was studied in Ref. [10] and led to the well-known family of dilatonic black holes. The solutions were indeed regular and asymptotically flat with the scalar field decreasing away from the horizon, in agreement with the above discussion. Here, we present the complimentary case with $f(\phi) = \alpha e^{-\phi}$ (the exact value of κ does not alter the physical characteristics of the solution, and, here, we set it to $\kappa = -1$). In the left plot of Fig. 1, we present a family of solutions for the scalar field ϕ for different initial values ϕ_h: for $\kappa = -1 < 0$, the scalar field must have ${\phi_h}' > 0$ and therefore increases as r increases. The value of the coupling constant α, once the form of the coupling function and the asymptotic value ϕ_h are chosen, is restricted by the inequality (22)—here, we present solutions for indicative allowed values of α.

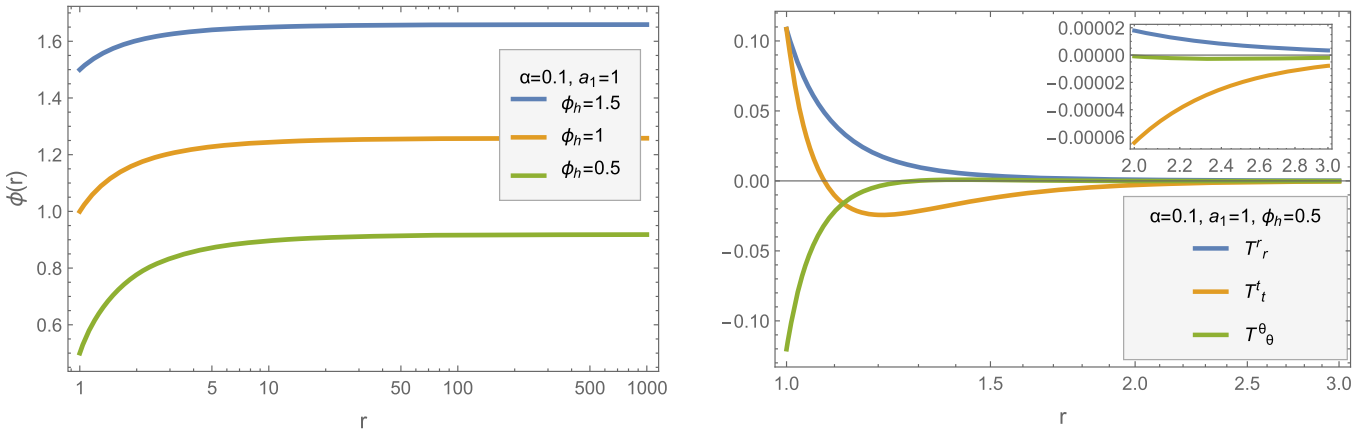

FIG. 1. The scalar field ϕ (left plot) and the energy-momentum tensor $T_{\mu\nu}$ (right plot) in terms of the radial coordinate r, for $f(\phi) = \alpha e^{-\phi}$.

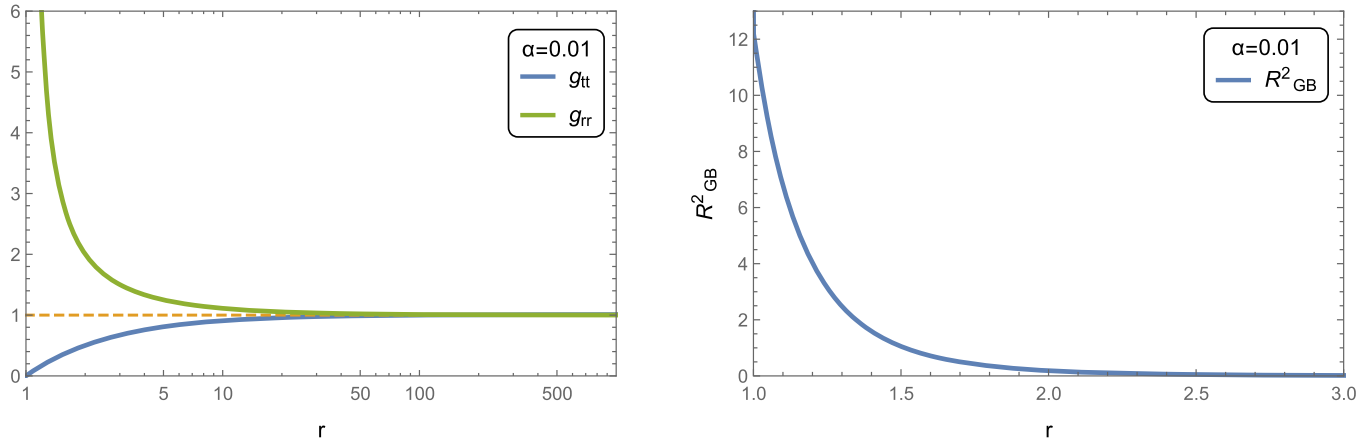

FIG. 2. The metric components g_{tt} and g_{rr} (left plot) and the Gauss-Bonnet term $R^2_{\rm GB}$ (right plot) in terms of the radial coordinate r, for $f(\phi) = \alpha e^{-\phi}$.

In the right plot of Fig. 1, we present the energy-momentum tensor components for an indicative solution of this family: clearly, all components remain finite over the whole radial regime. In particular, $T^r{}_r$ remains positive and monotonically decreases toward infinity, exactly the behavior that ensures the evasion of the novel no-hair theorem. As discussed in the previous section, apart from choosing the input value ϕ'_h for our numerical integration in accordance with Eq. (21), no other fine-tuning is necessary; the second constraint for the evasion of the novel no-hair theorem, i.e., $\dot{f}\phi'' + \ddot{f}\phi'^2 > 0$, is automatically satisfied without any further action, and this is reflected in the decreasing behavior of $T^r{}_r$ component near the horizon.

In the left and right plots of Fig. 2, we also present the solution for the two metric components $(|g_{tt}|, g_{rr})$ and the GB term $R^2_{\rm GB}$, respectively. The metric components exhibit the expected behavior near the black-hole horizon with g_{tt} vanishing and g_{rr} diverging at $r_h = 1$. To ensure asymptotic flatness at radial infinity, the free parameter a_1 appearing in the near-horizon solution (23) is appropriately chosen. On the other hand, the GB term remains finite and positive definite over the entire radial domain—in fact, it displays the monotonic behavior, hinted at by its two asymptotic limits (35) and (43), that causes the evasion of the old no-hair theorem. As expected, it contributes significantly near the horizon, where the curvature is large, and quickly fades away as we move toward larger distances. The profile of the metric components and GB term exhibit the same qualitative behavior in all families of black-hole solutions presented in this work, so we refrain from giving additional plots of these two quantities in the next subsections.

The profile of the scalar charge D as a function of the near-horizon value ϕ_h and of the mass M is given in the left and right plots, respectively, of Fig. 3 (each dot in these, and subsequent, plots stands for a different black-hole solution). For the exponential coupling function $f(\phi) = \alpha e^{-\phi}$, and for fixed α and r_h, the scalar field near the horizon ϕ_h may range from a minimum value, dictated by Eq. (22), up to infinity. As the left plot reveals, as $\phi_h \to \infty$, the coupling of the scalar field to the GB term vanishes, and we recover the Schwarzschild case with a trivial scalar field and a vanishing charge. On the other hand, in the right plot, we observe that as the mass of the black-hole increases the scalar charge decreases in

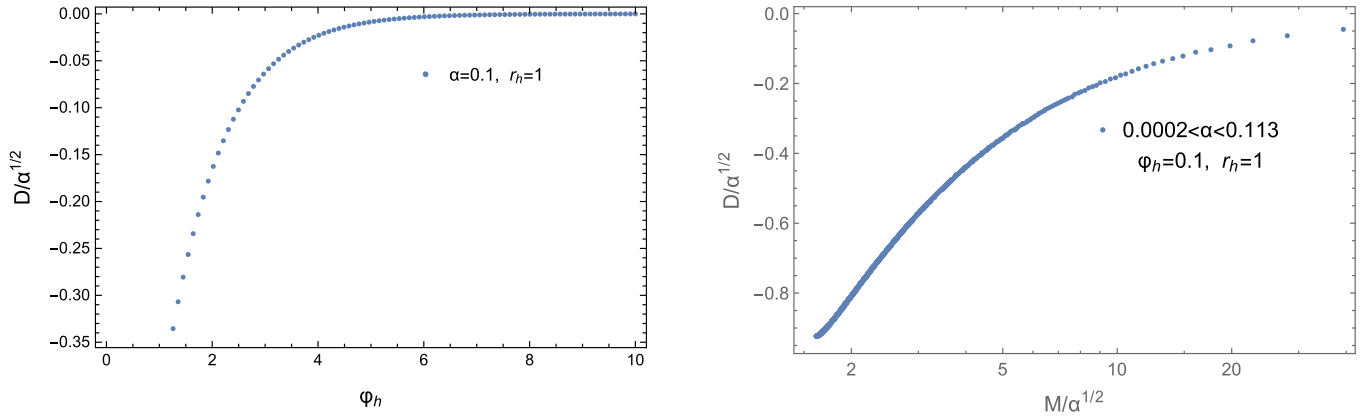

FIG. 3. The scalar charge D as a function of the near-horizon value ϕ_h (left plot) and of its mass M (right plot), for $f(\phi) = \alpha e^{-\phi}$.

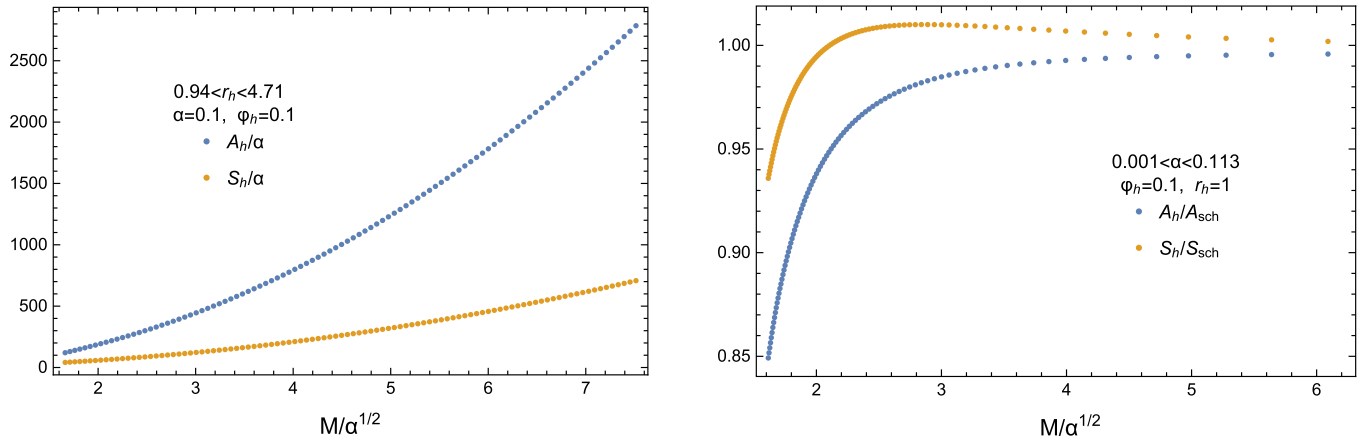

FIG. 4. The horizon area A_h and entropy S_h of the black hole (left plot) and their ratios to the corresponding Schwarzschild values (right plot) in terms of the mass M for $f(\phi) = \alpha e^{-\phi}$.

absolute value, and thus larger black holes tend to have smaller charges.

It is also interesting to study the profiles of the area of the black-hole horizon, $A_h = 4\pi r_h^2$, and of the entropy S_h of this class of solutions. The entropy is defined through the relation [32]

$$S_h = \beta\left[\frac{\partial(\beta F)}{\partial\beta} - F\right], \tag{45}$$

where $F = I_E/\beta$ is the Helmholtz free energy of the system given in terms of the Euclidean version of the action I_E. Also, $\beta = 1/(k_B T)$ with the temperature following easily from the definition [33,34]

$$T = \frac{k}{2\pi} = \frac{1}{4\pi}\left(\frac{1}{\sqrt{|g_{tt}g_{rr}|}}\left|\frac{dg_{tt}}{dr}\right|\right)_{r_h} = \frac{\sqrt{a_1 b_1}}{4\pi}. \tag{46}$$

The calculation of the temperature and entropy of the dilatonic black hole, with an exponential coupling function of the form $f(\phi) = \alpha e^{\phi}$, was performed in detail in Ref. [17]. By closely repeating the analysis, we find the expressions for the temperature,

$$T = \frac{1}{4\pi}\frac{(2M + D)}{r_h^2 + 4f(\phi_h)}, \tag{47}$$

and entropy,

$$S_h = \frac{A_h}{4} + 4\pi f(\phi_h), \tag{48}$$

of a GB black hole arising in the context of our theory (1) with a general coupling function $f(\phi)$ between the scalar field and the GB term. We easily confirm that, in the absence of the coupling function, the above quantities reduce to the corresponding Schwarzschild ones, $T = 1/(4\pi r_h)$ and $S_h = A_h/4$, respectively.

By employing the expressions for A_h and S_h as given above, we depict the horizon area and entropy, in terms of the mass of the black hole, in the left plot of Fig. 4; we observe that both quantities increase fast as the mass increases. The right plot allows us to compare more effectively our solutions to the Schwarzschild one. The lower curve depicts the ratio of A_h to the area of the Schwarzschild solution $A_{\rm Sch} = 16\pi M^2$, as a function of M; we observe that, for large black-hole masses, the ratio $A_h/A_{\rm Sch}$ approaches unity, and therefore, large GB black holes are not expected to deviate in their characteristics from the Schwarzschild solution of the same mass. On the other hand, in the small-mass limit, the ratio $A_h/A_{\rm Sch}$ significantly deviates from unity; in addition, a lower bound appears for the black-hole radius and thus of the mass of the black hole, due to the constraint (22) not present in the Schwarzschild case—this feature has been noted before in the case of the dilatonic black holes [10,25]. It is worth noting that the GB term, as an extra gravitational effect, causes the shrinking of the size of the black hole as the ratio $A_h/A_{\rm Sch}$ remains for all solutions below unity.

Turning finally to the entropy S_h of our black-hole solutions, we find a similar pattern: very small GB black holes differ themselves from the Schwarzschild solution by having a lower entropy, whereas large GB black holes tend to acquire, among other characteristics, also the entropy of the Schwarzschild solution. We observe, however, that, apart from the very small-mass regime close to the minimum value, the "exponential" GB black holes have in general a higher entropy than the Schwarzschild solution, a characteristic that points to the thermodynamical stability of these solutions. In fact, the dilatonic GB black holes [10], which comprise a subclass of this family of solutions with a coupling function of the form $f(\phi) = \alpha e^{\phi}$, have an identical entropy pattern and were shown to be linearly stable under small perturbations more than 20 years ago.

B. Even polynomial function

Next, we consider the case in which $f(\phi) = \alpha\phi^{2n}$, with $n \geq 1$. Since the coupling function must be positive definite, we assume again that $\alpha > 0$. The first constraint for the evasion of the novel no-hair theorem, $\dot{f}\phi' < 0$ near

the horizon, now translates to $\phi_h\phi'_h < 0$. Therefore, two classes of solutions appear for each value of n: one for $\phi_h > 0$, where $\phi'_h < 0$ and the solution for the scalar field decreases with r, and one for $\phi_h < 0$, where $\phi'_h > 0$ and the scalar field increases away from the black-hole horizon. In the left plot of Fig. 5, we depict the first family of solutions with $\phi_h < 0$ and $\phi'_h > 0$ for the choice $f(\phi) = \alpha\phi^2$, while in the left plot of Fig. 6, we depict the second class with $\phi_h > 0$ and $\phi'_h < 0$ for the choice $f(\phi) = \alpha\phi^4$. The complimentary classes of solutions may be easily derived in each case by reversing the signs of ϕ_h and ϕ'_h.

The form of the energy-momentum tensor components for the two choices $f(\phi) = \alpha\phi^2$ and $f(\phi) = \alpha\phi^4$, and for two indicative solutions, are depicted in the right plots of Figs. 5 and 6, respectively. We observe that the qualitative behavior of the three components largely remains the same, despite the change in the form of the coupling function $f(\phi)$ (note also the resemblance with the behavior depicted in the right plot of Fig. 1). In fact, the asymptotic behavior of $T_{\mu\nu}$ near the black-hole horizon and radial infinity is fixed, according to Eqs. (29)–(31) and (42), respectively. Independently of the form of the coupling function $f(\phi)$, at asymptotic infinity, $T^r{}_r$ approaches zero from the positive side, while $T^t{}_t$ and $T^\theta{}_\theta$ do the same from the negative side. In the near-horizon regime, Eqs. (29)–(31) dictate that

$$\mathrm{sign}(T^t{}_t)_h, \qquad \mathrm{sign}(T^r{}_r)_h \sim -\mathrm{sign}(\phi'_h\dot{f}_h), \tag{49}$$

$$\mathrm{sign}(T^\theta{}_\theta)_h \sim +\mathrm{sign}(\phi'_h\dot{f}_h). \tag{50}$$

Using that $\dot{f}_h\phi'_h < 0$ and the scaling behavior of the metric functions near the horizon, we may easily derive that $(T^t{}_t)_h$ and $(T^r{}_r)_h$ always assume positive values while $(T^\theta{}_\theta)_h$ assumes a negative one. The form of $f(\phi)$ merely changes the magnitude of these asymptotic values: in the case of a polynomial coupling function, the higher the degree is, the larger the asymptotic values near the horizon are.

One could assume that the intermediate behavior of the scalar field and the energy-momentum tensor always remains qualitatively the same. In fact, this is not so. Let us fix for simplicity the values of r_h and ϕ_h and gradually increase the value of the coupling parameter α;

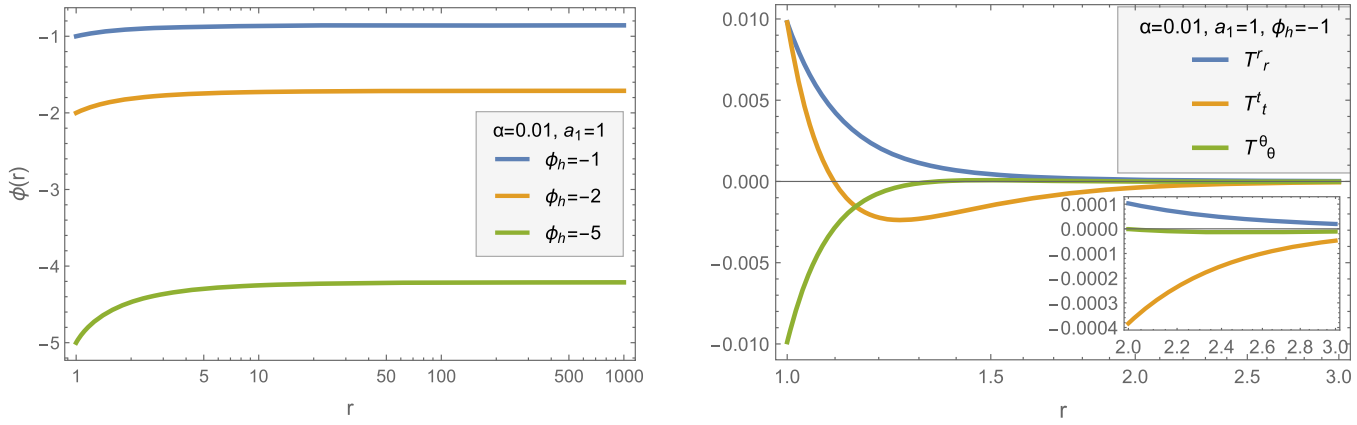

FIG. 5. The scalar field ϕ (left plot) and the energy-momentum tensor $T_{\mu\nu}$ (right plot) in terms of the radial coordinate r, for $f(\phi) = \alpha\phi^2$.

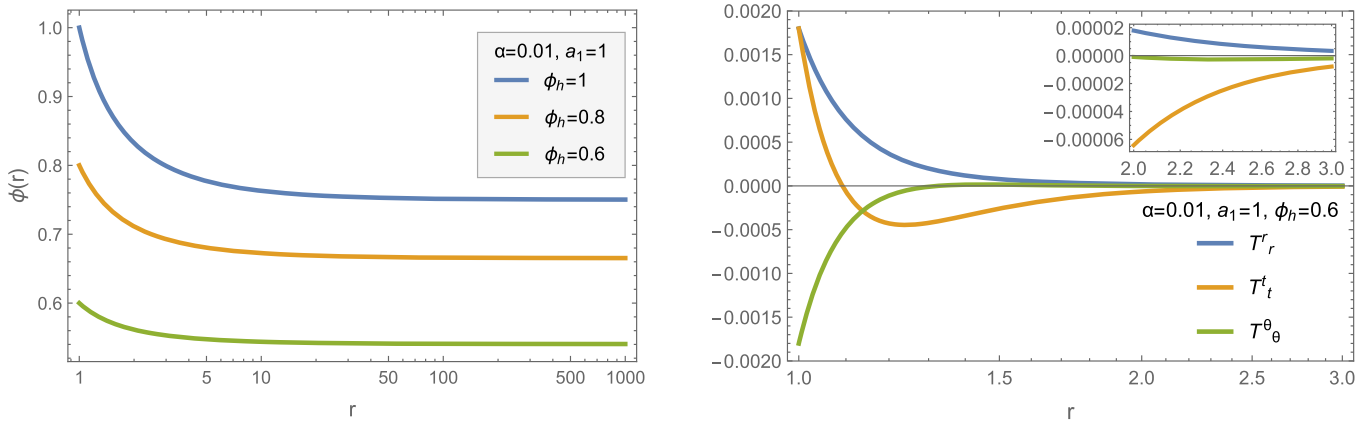

FIG. 6. The scalar field ϕ (left plot) and the energy-momentum tensor $T_{\mu\nu}$ (right plot) in terms of the radial coordinate r, for $f(\phi) = \alpha\phi^4$.

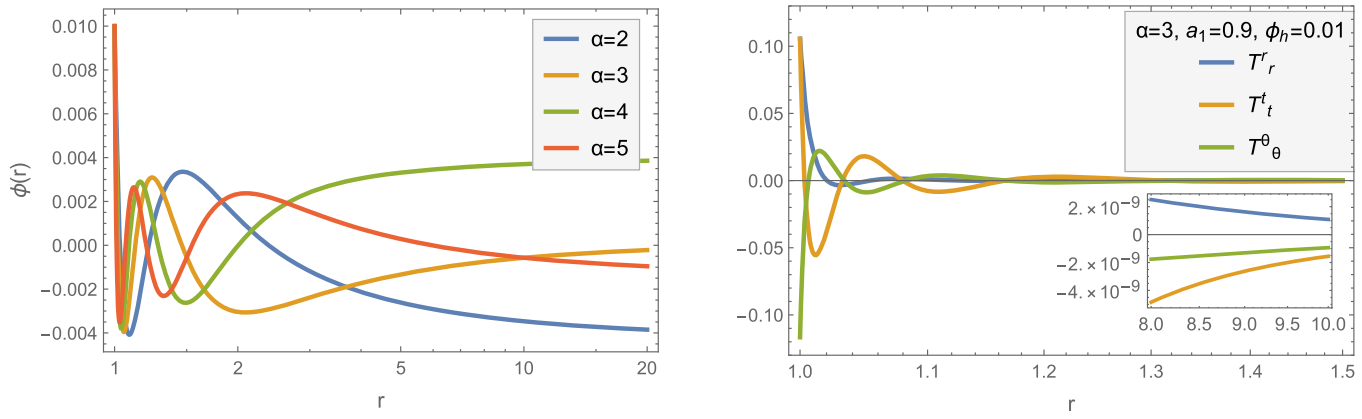

FIG. 7. The scalar field ϕ (left plot) and the energy-momentum tensor $T_{\mu\nu}$ (right plot) in terms of the radial coordinate r, for $f(\phi) = \alpha\phi^2$ and various values of the coupling constant α.

this has the effect of increasing the magnitude of the GB source term appearing in the equation of motion (4) for ϕ. For an indicative case, in the left plot of Fig. 7, we depict the behavior of ϕ for four large values of α, and in the right plot, we depict the behavior of $T_{\mu\nu}$ for one of these solutions. We observe that all of these quantities are not monotonic anymore; they go through a number of maxima or minima—with that number increasing with the value of α—before reaching their asymptotic values at infinity. Note that the near-horizon behavior of both ϕ and $T_{\mu\nu}$ is still the one that guarantees the evasion of the no-hair theorem. We may thus conclude that the presence of the GB term in the theory not only ensures that the asymptotic solutions (23)–(25) and (36)–(38) may be smoothly connected to create a regular black hole, but it allows for this to happen even in a nonmonotonic way.

Let us also study the characteristics of this class of black-hole solutions arising for an even polynomial coupling function. In Fig. 8 (left plot), we depict the scalar charge D in terms of the mass M of the black hole, for the quadratic coupling function $f(\phi) = \alpha\phi^2$: we observe that, in this case, the function $D(M)$ is not monotonic in the small-mass regime but it tends again to zero for large values of its mass. In terms of the near-horizon value ϕ_h, the scalar charge exhibits the expected behavior: for large values of ϕ_h, the effect of the GB term becomes important and D increases; on the other hand, for vanishing ϕ_h, i.e., a vanishing coupling function, the scalar charge also vanishes (in order to minimize the number of figures, we refrain from showing plots depicting the anticipated behavior). In the same spirit, we present no new plots for the quartic coupling function as it leads to exactly the same qualitative behavior.

Turning to the horizon area A_h and entropy S_h of these black-hole solutions, we find that, in terms of the mass M, they both quickly increase, showing a profile similar to that of Fig. 4 (left plot) for the exponential case. The ratio $A_h/A_{\rm Sch}$ remains again below unity over the whole mass regime and interpolates between a value corresponding to the lowest allowed value of the mass, according to Eq. (22), and the asymptotic Schwarzschild value at the large-mass limit. The entropy ratio $S_h/S_{\rm Sch}$, on the other hand, is found to have a different profile by remaining now always below unity—this feature points perhaps toward a thermodynamic instability of the "even polynomial" GB black holes compared to the Schwarzschild solution.

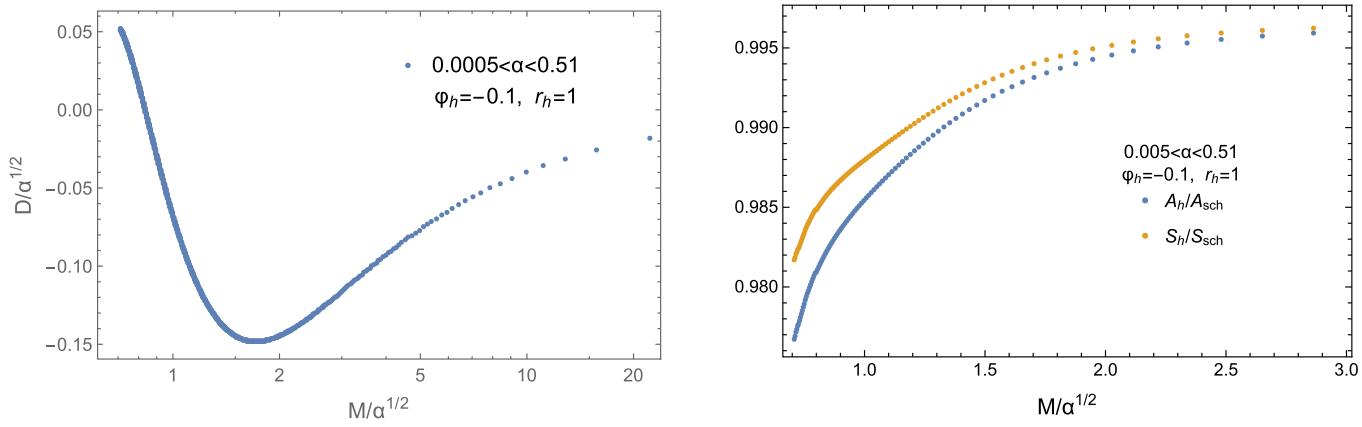

FIG. 8. The scalar charge D (left plot) and the ratios $A_h/A_{\rm Sch}$ and $S_h/S_{\rm Sch}$ (right plot) in terms of the mass M, for $f(\phi) = \alpha\phi^2$.

C. Odd polynomial function

We now consider the case of $f(\phi) = \alpha\phi^{2n+1}$, with $n \geq 0$ and $\alpha > 0$. Here, the constraint $\dot{f}\phi' < 0$ translates to $\phi^{2n}\phi' < 0$, or simply to $\phi'_h < 0$ for all solutions. In Fig. 9, we have chosen the linear case, i.e., $f(\phi) = \alpha\phi$, and presented an indicative family of solutions for the scalar field (left plot) and the components of the energy-momentum tensor for one of them (right plot). The decreasing profile of ϕ for all solutions, as we move away from the black-hole horizon, is evident and in agreement with the above constraint. The energy-momentum tensor clearly satisfies the analytically predicted behavior at the two asymptotic regimes, which once again ensures the evasion of the novel no-hair theorem.

The two plots in Fig. 10, left and right, depict the same quantities but for the case $f(\phi) = \alpha\phi^3$. Their profile agrees with that expected for a regular, black-hole solution with a scalar hair. The alerted reader may notice that, here, we have chosen to present solutions with $\phi_h < 0$; for an odd polynomial coupling function, these should have been prohibited under the constraint $f(\phi) > 0$, which follows from the old no-hair theorem [3,31]. Nevertheless, regular black-hole solutions with a nontrivial scalar field that do not seem to satisfy $f(\phi) > 0$ do emerge. A set of such solutions is shown in the left plot of Fig. 10 (we refrain from showing the set of solutions with $\phi_h > 0$ as these have similar characteristics). As we observe, all of them obey the $\phi'_h < 0$ constraint imposed by the evasion of the novel no-hair theorem and lead to the expected behavior of $T_{\mu\nu}$; the latter may be clearly seen in the right plot of Fig. 10 in which such a "prohibited" solution is plotted. The behavior of the metric components and the GB term continue to be given by plots similar to the ones in Fig. 2.

The emergence of solutions that violate the constraint $f(\phi) > 0$ is in fact a general feature of our analysis and not an isolated finding in the case of the odd polynomial coupling function. Apparently, the presence of the coupling of the scalar field to the GB term not only opens the way for black-hole solutions to emerge but renders the old no-hair theorem incapable of dictating when this may happen. Looking more carefully at the argument on which the old no-hair theorem was based in Refs. [3,31], one readily

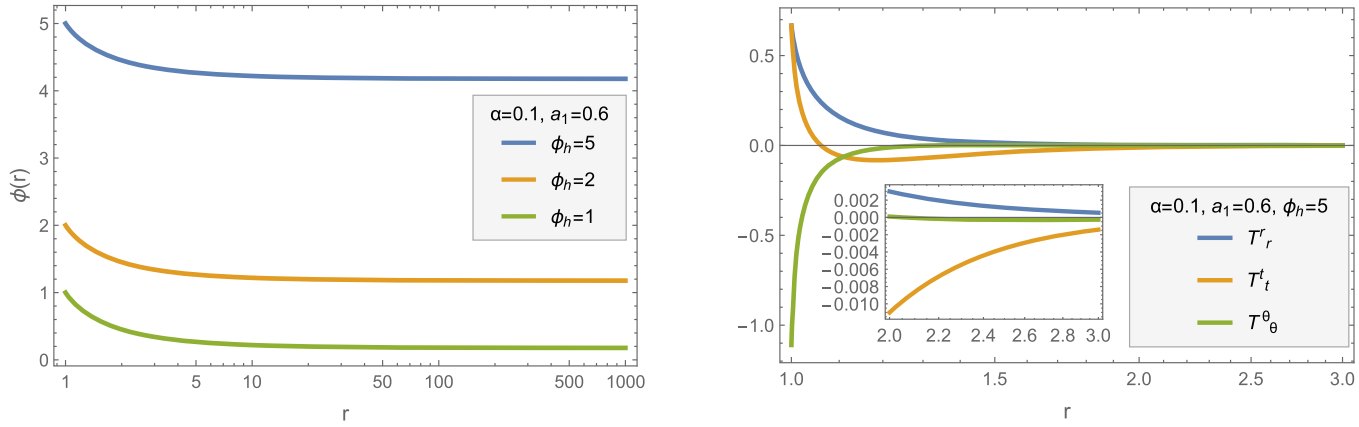

FIG. 9. The scalar field ϕ (left plot) and the energy-momentum tensor $T_{\mu\nu}$ (right plot) in terms of the radial coordinate r, for $f(\phi) = \alpha\phi$.

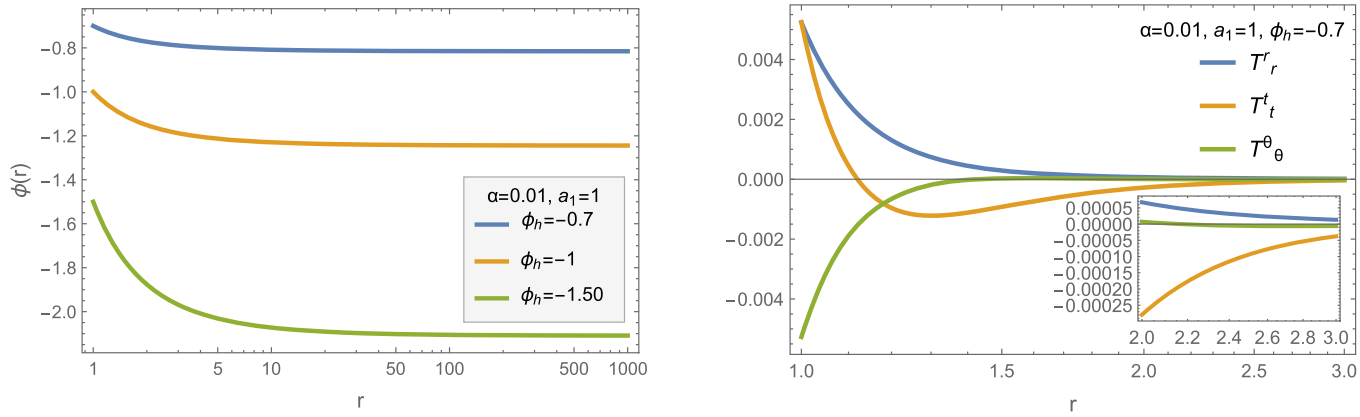

FIG. 10. The scalar field ϕ (left plot) and the energy-momentum tensor $T_{\mu\nu}$ (right plot) in terms of the radial coordinate r, for $f(\phi) = \alpha\phi^3$.

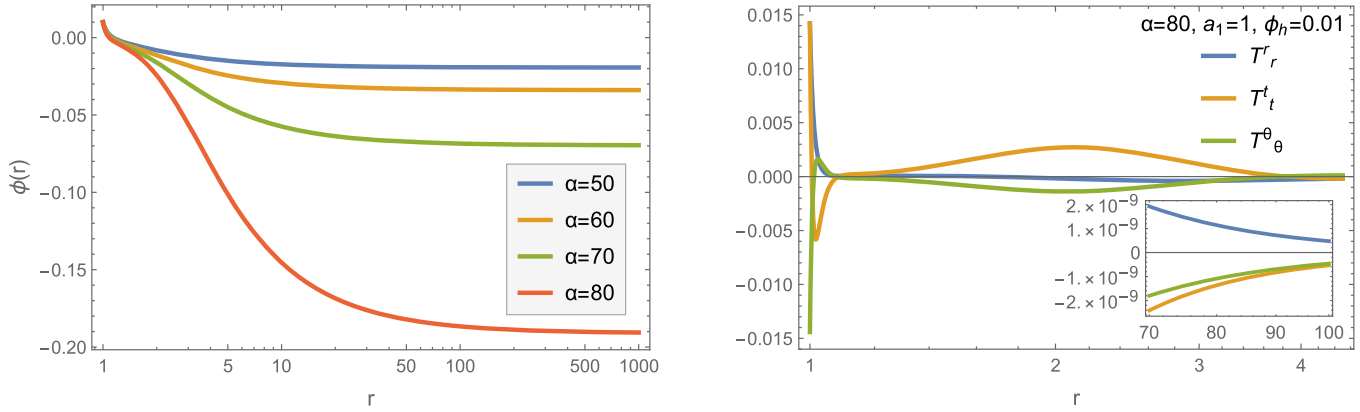

FIG. 11. The scalar field ϕ (left plot) and the energy-momentum tensor $T_{\mu\nu}$ (right plot) in terms of the radial coordinate r, for $f(\phi) = \alpha\phi^3$ and a variety of values of the coupling constant α.

realizes that this involves the integral of the scalar equation over the entire exterior regime and thus the global solution of the field equations of which the characteristics cannot be predicted beforehand. In contrast, the evasion of the novel no-hair theorem is based on local quantities, such as the energy-momentum components and their derivatives at particular radial regimes, which may be easily computed. In addition, this is indifferent to the behavior of the solution in the intermediate regime, which may indeed exhibit an arbitrary profile as the one presented in the plots of Fig. 7. In fact, all solutions found in the context of our analysis, with no exception, satisfy the constraints that ensure the evasion of the novel no-hair theorem.

In this case, too, one may derive solutions for a variety of values of the coupling constant α, as long as these obey the constraint (22). In Fig. 11 (left plot), we depict a family of solutions with $\phi_h = 0.01$ and a variety of values of α. This family of solutions presents a less monotonic profile compared to the one exhibited by the solutions in Fig. 10. The components of the energy-momentum tensor for one of these solutions are depicted in the right plot of Fig. 11, and they present a more evolved profile with the emergence of minima and maxima between the black-hole horizon and radial infinity. We also notice that the solutions for the scalar field, although they start from the positive-value regime ($\phi_h = 0.01$), cross to negative values for fairly small values of the radial coordinate. This behavior causes the odd coupling function to change sign along the radial regime, a feature that makes any application of the old no-hair theorem even more challenging.

Turning again to the characteristics of the "odd polynomial" black-hole solutions, in Fig. 12 (left plot), we depict the scalar charge D in terms of the mass M of the black hole, for the linear coupling function $f(\phi) = \alpha\phi$: here, the function $D(M)$ is monotonic and approaches a vanishing asymptotic value as M increases. The scalar charge D has no dependence on the initial scalar-field value ϕ_h since it is the first derivative $f'(\phi)$ that appears in the scalar equation (4) and, for a linear function, this is merely a constant. The horizon area A_h and entropy S_h exhibit again an increasing profile in terms of M similar to that of Fig. 4 (left plot) for the exponential case. The more informative ratios $A_h/A_{\rm Sch}$ and $S_h/S_{\rm Sch}$ are given in the right plot of Fig. 12: as in the case of quadratic and quartic coupling functions, both quantities remain smaller than unity and interpolate between a lowest value corresponding to the

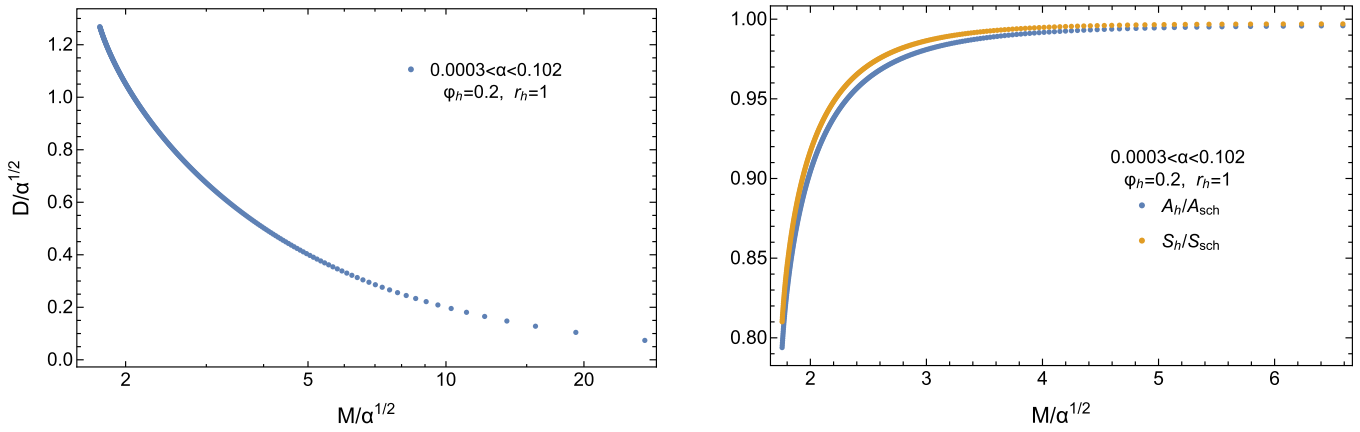

FIG. 12. The scalar charge D (left plot) and the ratios $A_h/A_{\rm Sch}$ and $S_h/S_{\rm Sch}$ (right plot) in terms of the mass M, for $f(\phi) = \alpha\phi$.

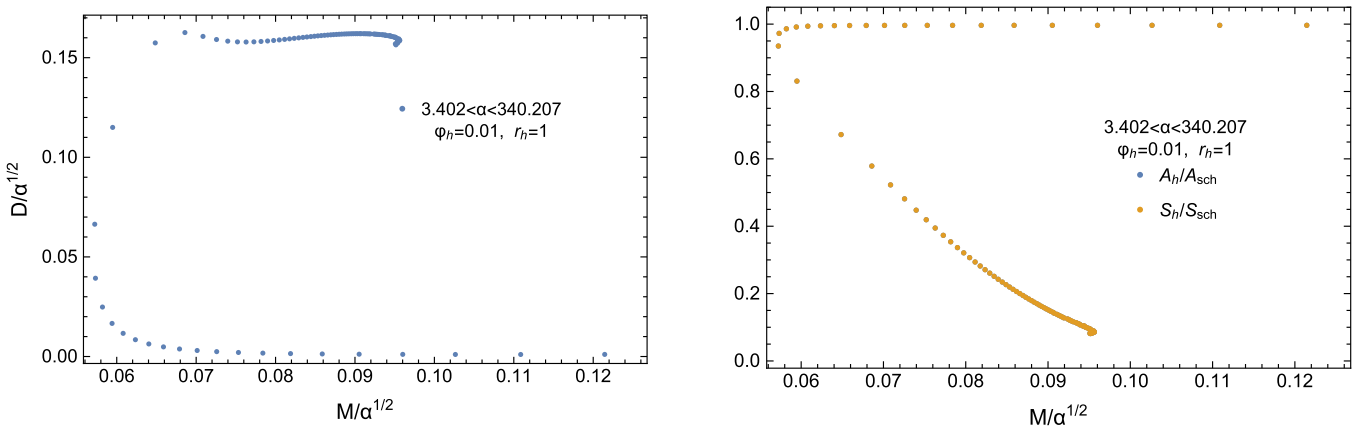

FIG. 13. The scalar charge D (left plot) and the ratios $A_h/A_{\rm Sch}$ and $S_h/S_{\rm Sch}$ (right plot) in terms of the mass M, for $f(\phi) = \alpha\phi^3$.

black-hole solution with the lowest mass and the Schwarzschild limit acquired at the large mass limit.

We now separately address the characteristics of the black-hole solutions arising in the case of the cubic coupling function $f(\phi) = \alpha\phi^3$ since here we find a distinctly different behavior. As mentioned above, also in this case, as the coupling constant α increases, from zero to its maximum value (for r_h and ϕ_h fixed), solutions with no monotonic profile in terms of the radial coordinate arise (see the left plot of Fig. 11). We depict the scalar charge D in terms of the mass M of the black hole, for the whole α regime, in the left plot of Fig. 13; we may easily observe the emergence of two different branches of solutions (with a third, short one appearing at the end of the upper branch) corresponding to the same mass M. These branches appear at the small-mass limit of the solutions, whereas for large masses, only one branch survives with a very small scalar charge. In the right plot of Fig. 13, we show the ratio $S_h/S_{\rm Sch}$ in terms of the mass M; this quantity also displays the existence of three branches with the one that is smoothly connected to the Schwarzschild limit having the higher entropy. The two additional branches with the larger values of scalar charge, compared to the one of the "Schwarzschild" branch, have a lower entropy, and they are probably less thermodynamically stable. This behavior was not observed in the case of the quadratic coupling function in which more evolved solutions for the scalar field also appeared (see the left plot of Fig. 5): there, the function $D(M)$ was not monotonic but was always single valued. That created short, disconnected "branches" of solutions with slightly different values of entropy ratio $S_h/S_{\rm Sch}$ but all lying below unity. Let us finally note that the horizon area ratio $A_h/A_{\rm Sch}$, not shown here for brevity, has the same profile as the one displayed in Fig. 12 for the linear function, while the $D(\phi_h)$ function shows the anticipated increasing profile as ϕ_h, and thus the GB coupling, increases.

D. Inverse polynomial function

The next case to consider is the one in which $f(\phi) = \alpha\phi^{-k}$, where $k > 0$, and α is also assumed to be positive, for simplicity. Let us consider directly some indicative cases:

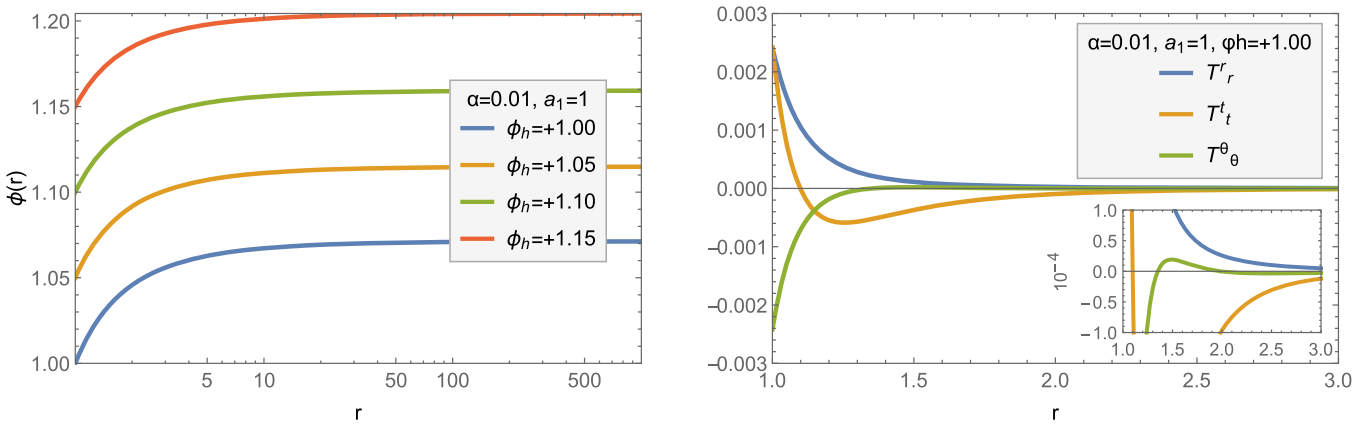

FIG. 14. The scalar field ϕ (left plot) and the energy-momentum tensor $T_{\mu\nu}$ (right plot) in terms of the radial coordinate r, for $f(\phi) = \alpha/\phi$.

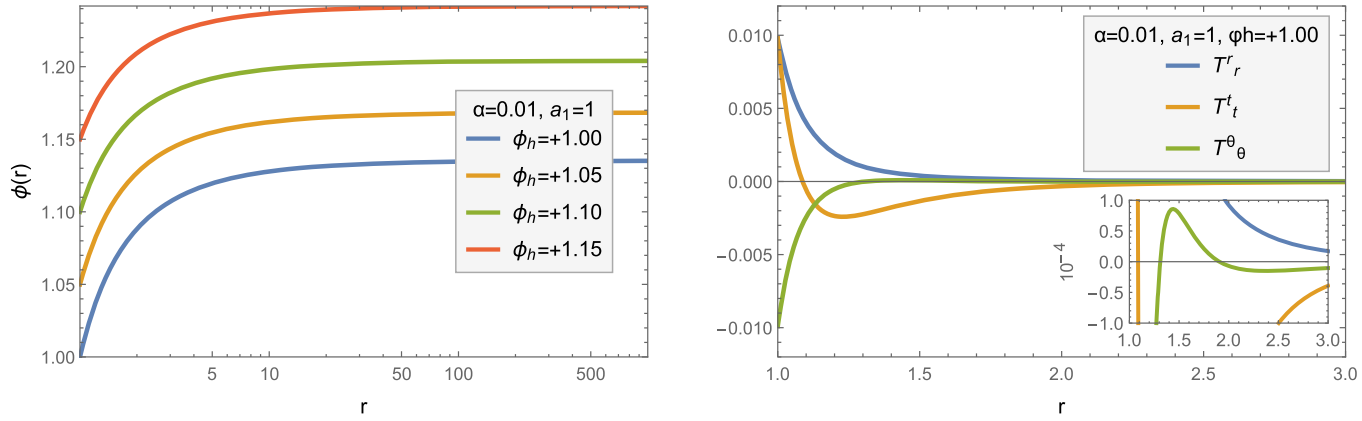

FIG. 15. The scalar field ϕ (left plot) and the energy-momentum tensor $T_{\mu\nu}$ (right plot) in terms of the radial coordinate r, for $f(\phi) = \alpha/\phi^2$.

(i) $k = 1$: In this case, the constraint for the evasion of the novel no-hair theorem becomes $\dot{f}\phi' = -2\alpha\phi'/\phi^2 < 0$, which demands $\phi'_h > 0$ for all solutions. At the left plot of Fig. 14, we present a family of solutions for the scalar field emerging for this coupling function. All solutions are increasing away from the black-hole horizon in accordance to the above comment. The components of the energy-momentum tensor are also well behaved, as may be seen from the right plot of Fig. 14. As in the case of the odd polynomial function, an additional set of solutions arises with $\phi_h < 0$ with similar characteristics.

(ii) $k = 2$: In this case, the constraint becomes $\dot{f}\phi' = -\alpha\phi'/\phi^3 < 0$, which demands $\phi_h\phi'_h > 0$. A family of solutions for the scalar field emerging for this coupling function, with $\phi_h > 0$ and increasing with r, is presented at the left plot of Fig. 15—a complementary family of solutions with $\phi_h < 0$ and decreasing away from the black-hole horizon was also found. The components of the energy-momentum tensor for an indicative solution are depicted at the right plot of Fig. 15 and clearly remain finite over the whole exterior regime.

Concerning the characteristics of the "inverse polynomial" GB black holes, we find again interesting behavior—in Fig. 16, we depict the inverse linear case, as an indicative one. The scalar charge D exhibits a monotonic decreasing behavior in terms of the mass M, as one may see in the left plot of the figure, approaching zero at the large-mass limit. In terms of the input parameter ϕ_h, the scalar charge presents the anticipated behavior (and thus is not shown here): for an inverse coupling function, D increases as the value of ϕ_h, and thus of the GB coupling, decreases. The quantities A_h and S_h increase once again quickly with the mass M, as in Fig. 4. The ratio $A_h/A_{\rm Sch}$ is shown in the right plot of Fig. 16 and reveals again the constantly smaller size of the GB black holes compared to the asymptotic Schwarzschild solution as well as the existence of a lowest-mass solution. The ratio $S_h/S_{\rm Sch}$, depicted also in Fig. 16, reveals that the entire class of these black-hole solutions—independently of their mass—has a higher entropy compared to the asymptotic Schwarzschild solution. This feature is in fact unique for the inverse linear function; a

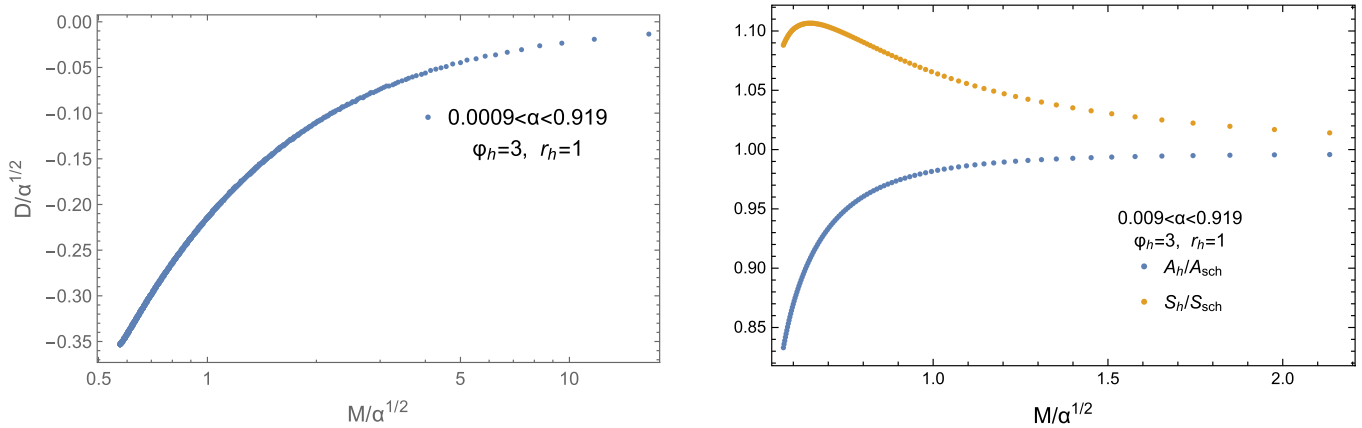

FIG. 16. The scalar charge D (left plot) and the ratios $A_h/A_{\rm Sch}$ and $S_h/S_{\rm Sch}$ (right plot) in terms of the mass M, for $f(\phi) = \alpha/\phi$.

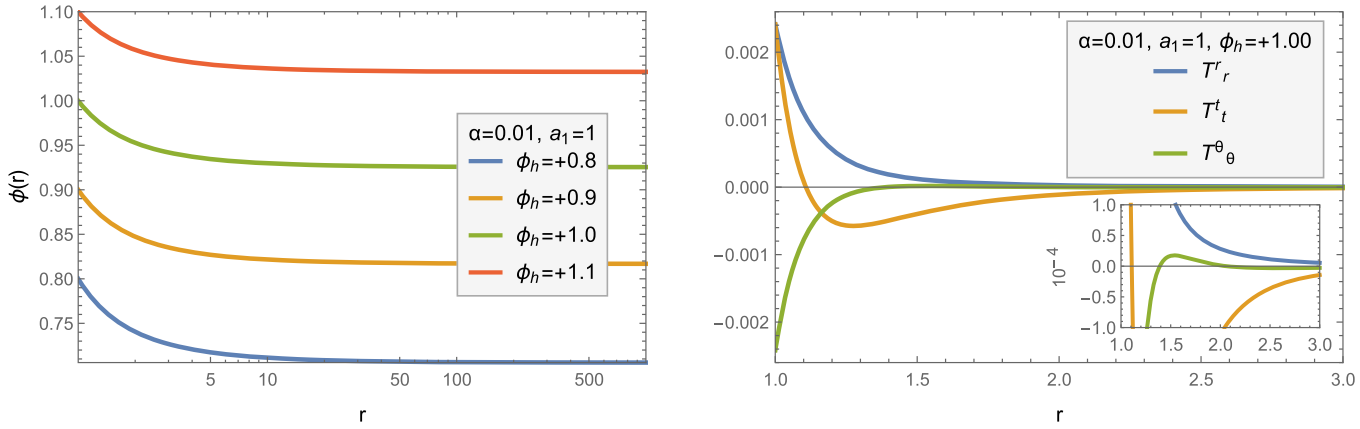

FIG. 17. The scalar field ϕ (left plot) and the energy-momentum tensor $T_{\mu\nu}$ (right plot) in terms of the radial coordinate r, for $f(\phi) = \alpha \ln \phi$.

similar analysis for the inverse quadratic coupling function has produced similar results for the quantities $D(M)$, $D(\phi_h)$, $A_h/A_{\rm Sch}$, and $S_h/S_{\rm Sch}$ with the only difference being that the very-low-mass regime of the "inverse quadratic" GB black holes has a lower entropy than the Schwarzschild solution; i.e., the situation resembles more the one depicted in Fig. 4.

E. Logarithmic function

We finally address the case in $f(\phi) = \alpha \ln(\phi)$. Here, black-hole solutions emerge for $\dot{f}\phi' = \alpha\phi'/\phi < 0$, near the black-hole horizon; for $\alpha > 0$, this translates to $\phi'_h < 0$ (since the argument of the logarithm must be a positive number, i.e., $\phi > 0$). As a result, the solutions for the scalar field are restricted to having a decreasing behavior as we move away from the black-hole horizon—this is indeed the behavior observed in the class of solutions depicted in the left plot of Fig. 17. One may also observe that the plot includes solutions with either $\phi_h > 1$ or $\phi_h < 1$, or equivalently with $f > 0$ or $f < 0$. Once again, the old no-hair theorem is proven to be inadequate to exclude the presence of regular black holes with scalar hair even in subclasses of the theory (1). In contrast, the derived solutions continue to satisfy the constraints for the evasion of the novel no-hair theorem.

The components of the energy-momentum tensor are presented in the right plot of Fig. 17: they exhibit the same characteristics as in the cases presented in the previous subsections with the most important being the monotonic, decreasing profile of the $T^r{}_r$ component. The coupling constant α can also take a variety of values as long as it satisfies Eq. (22); in this case, the monotonic behavior of ϕ over the whole exterior space of the black hole is preserved independently of the value of α. The energy-momentum tensor also assumes the same form as in Fig. 17, and thus we refrain from presenting any new plots.

The scalar charge D of the "logarithmic" GB black holes in terms of the mass M is shown in the left plot of Fig. 18. Once again, we observe that, as the mass of the black-hole solution increases, D decreases toward a vanishing value—our previous analysis has shown that this feature is often connected with the thermodynamical stability of the solutions. Indeed, as it may be seen from the right plot of

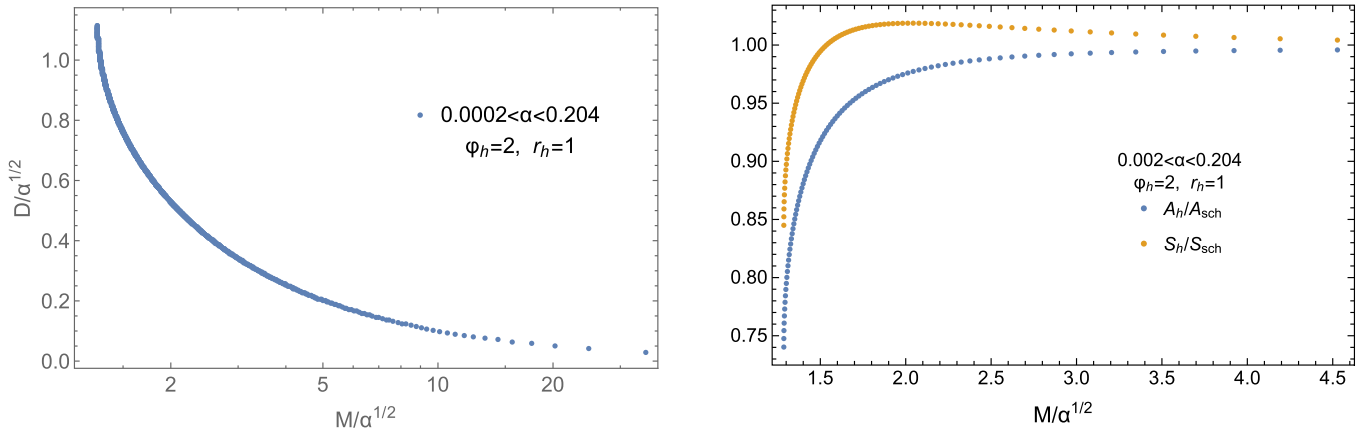

FIG. 18. The scalar charge D (left plot) and the ratios $A_h/A_{\rm Sch}$ and $S_h/S_{\rm Sch}$ (right plot) in terms of the mass M, for $f(\phi) = \alpha \ln \phi$.

Fig. 18, the ratio $S_h/S_{\rm Sch}$ is above unity for a very large part of the mass regime; it is again the small-mass regime that is excluded from the thermodynamical stable solutions. The scalar charge D has again the anticipated behavior in terms of the parameter ϕ_h: since it is the $f'(\phi) = \alpha/\phi$ that enters the scalar equation (4), the scalar charge increases as ϕ_h decreases. The ratio $A_h/A_{\rm Sch}$ is also shown in the right plot of Fig. 18; as in the previous cases, it corresponds to a class of smaller black-hole solutions, compared to the Schwarzschild solution of the same mass, with a minimum-allowed mass that approaches the asymptotic Schwarzschild solution as M reaches large values.

IV. CONCLUSIONS

The emergence of regular black-hole solutions in theories with scalar fields has always attracted the interest of researchers especially in conjunction with the no-hair theorems. The latter were formed in an attempt to limit the emergence of black-hole solutions in the context of theories beyond General Relativity. However, a small number of theories, in which the evasion of those theorems was realized, have been found in the literature over the years, leading to novel solutions with scalar hair.

A main characteristic of those theories was the coupling of the scalar field with higher-order gravitational terms. When one focuses on theories in which the higher-curvature term is the quadratic Gauss-Bonnet term, the number of black-hole solutions with nontrivial scalar hair, which have been found in the literature, is very limited [10,28]. These two works considered the particular cases of a string-inspired, exponential coupling function between the scalar field and the GB term and a shift-symmetric linear coupling function, respectively. In a previous work of ours [31], we nevertheless demonstrated that regular black-hole solutions with scalar hair may be constructed in the context of a much more general class of theories that contain the GB term. For this to be realized and the theory to evade the no-hair theorems, the general coupling function $f(\phi)$ had to satisfy two constraints. The first constraint was imposed on the value of ϕ_h'; this uniquely determined this quantity that could then be used as an input parameter for the construction of the solutions. Using this, we were indeed able to produce asymptotically flat, regular black-hole solutions; these were briefly presented in Ref. [31].

In the present work, we have extended the analysis of Ref. [31] by considering several subclasses of the general theory that contained the Ricci scalar, a scalar field, and the GB term. We have studied a large number of choices for the coupling function $f(\phi)$ between the scalar field and the GB term: exponential, polynomial (even and odd), inverse polynomial (even and odd), and logarithmic. In each case, employing the constraint (21) for the value of ϕ_h', we constructed a large number of exact black-hole solutions with scalar hair and studied in detail their characteristics. Our solutions were characterized by a universal behavior of the components of the metric tensor, having the expected behavior near the black-hole horizon and asymptotic flatness at radial infinity. All curvature-invariant quantities were examined and found to have a similar universal profile, independently of the form of the coupling function f, which ensured the finiteness of the spacetime and thus the regularity of all solutions.

The same regularity characterized the components of the energy-momentum tensor over the whole radial regime. In fact, the first constraint on the value of ϕ_h'—necessary for the evasion of the novel no-hair theorem—simultaneously guarantees the regularity of the scalar field at the black-hole horizon and therefore the regularity of the solution. The second constraint for the evasion of the no-hair theorem involves both ϕ_h' and ϕ_h'' and determines the behavior of $T^r{}_r$ near the black-hole horizon; this constraint was automatically satisfied by all the constructed solutions and demanded no further action or fine-tuning of the parameters. It is worth noting that these constraints were local as they applied to the black-hole radial regime and were therefore easy to check. On the other hand, the old no-hair theorem, based on an integral constraint over the whole radial regime, failed to lead to a unique constraint, the violation or not of which would govern the existence of regular black-hole solutions. A special form of it, i.e., $f(\phi) > 0$, was found to lead, indeed, to novel solutions when satisfied, but it could not exclude their emergence in the opposite case.

The profile for the scalar field ϕ was found in all of the cases considered and was indeed regular over the entire radial domain. The scalar field increased or decreased away from the black-hole horizon, always in accordance with the constraint (21), and approached a constant value at asymptotic infinity. The scalar charge D was determined in each case, and its dependence on either ϕ_h or M was studied. In terms of the first parameter, the value of which determines the magnitude of the GB coupling in the theory, its behavior was the anticipated one: for large values of that coupling, D assumed a large value, while for small couplings, D tended to zero. Its profile in terms of the mass M of the black hole had a universal behavior in the large-M limit, with D assuming increasingly smaller values; however, in the small-M limit, each family of solutions presented a different behavior (either monotonic or not monotonic). In all cases, however, the scalar charge is an M-dependent quantity, and therefore our solutions have a nontrivial scalar field but with a "secondary" hair.

The horizon area A_h and entropy S_h of the solutions were also found in each case. Both quantities quickly increased with the mass M, with the former always dominating over the latter. The function $A(M)$ also revealed a generic feature of all black-hole solutions found, namely, the existence of a lower value for the horizon radius r_h and thus of the horizon area A_h of the black hole; this was due to the constraint (22)

that, for fixed ϕ_h and parameter α, did not allow for regular solutions with horizon radius smaller than a minimum value, given by $(r_h^2)_{\rm min} = 4\sqrt{6}|\dot{f}_h|$, to emerge. This, in turn, imposed a lower-bound on the mass of the black-hole solution, and therefore all curves $A(M)$ terminated at a specific point in the low-mass regime.

The study of the ratios $A_h/A_{\rm Sch}$ and $S_h/S_{\rm Sch}$, with respect to the corresponding quantities of the Schwarzschild solution with the same mass, had even more information to offer. The first ratio remained below unity for all classes of black-hole solutions found and for all mass regimes; as a result, we may conclude that the presence of the additional, gravitational GB term leads to the formation of more compact black holes compared to the standard General Relativity. In the large-mass limit, the horizon area of all black-hole solutions approached the Schwarzschild value—the same was true for the entropy ratio $S_h/S_{\rm Sch}$; these two features together suggest that, for large masses, it will be extremely difficult to distinguish between GB black holes and their General Relativity analogs.

Do we really expect to detect any of these classes of GB black holes in the Universe? This depends first on their stability behavior, a topic that needs to be studied carefully and individually for each class of solutions presented in this work. The curves $S_h/S_{\rm Sch}(M)$, which we produced, may provide hints for their stability: as mentioned above, the entropy of all solutions found here approached, in the large-M limit, the Schwarzschild value, and thus it is quite likely that large GB black holes share the stability of the Schwarzschild solution. For smaller masses, in which the GB black holes are expected to differ from their GR analog, different profiles were observed: the "exponential," inverse-quadratic, and logarithmic GB black holes had a ratio $S_h/S_{\rm Sch}$ larger than unity for the entire intermediate mass regime but smaller than unity in the very-low-mass regime. These results point toward the thermodynamical stability of solutions with intermediate and large masses but to an instability for solutions with small masses [although, even in the latter case, an accretion of mass from their environment could lead to an increase in their mass and to a change in their (in)stability]. On the other hand, the "quadratic," "quartic," and "linear" GB black holes had their entropy ratio $S_h/S_{\rm Sch}$ below unity over the entire mass regime and perhaps did not lead to stable configurations. Finally, two classes of solutions, the "inverse-linear" and the first branch of the "cubic" GB black holes have their ratio $S_h/S_{\rm Sch}$ larger than unity for all values of the black-hole mass—small, intermediate, and large—and may hopefully lead to stable solutions with a variety of masses. In all cases, a careful study of all the above solutions under perturbations is necessary in order to verify or refute the above expectations (the only class of GB black-hole solutions that has been studied under linear perturbations are the exponential ones that were found to be indeed stable [10] in accordance with the above comments).

Assuming therefore that one or more classes of the aforementioned black-hole solutions are stable, we then need a number of signatures or observable effects that would distinguish them from their GR analogs and convince us of their existence. A generic feature of all GB black holes is their minimum horizon radius: if, in the small-mass limit, certain families of GB black holes are more favorable to emerge compared to the Schwarzschild solution—from the stability point of view, then, the observed black holes will not have an arbitrarily small mass. Also, in the small-mass limit, observable effects may include deviations from standard GR in the calculation of the bending angle of light, the precession observed in near-horizon orbits, and the spectrum from their accretion discs. Studies of this type have been performed [35] for black holes in the Einstein-scalar-GB theory with a linear coupling [26]—a special case of our analysis—and shown that the near-horizon strong dynamics may leave its imprint on all of these observables.

Our GB black-hole solutions are characterized also by a scalar charge. A previous analysis of dilatonic (exponential) GB black holes [36] has revealed that scalar radiation is rather suppressed, especially for nonspinning black holes, unless particular couplings are introduced in the theory between the scalar field and ordinary matter. In addition, in Ref. [37], it was demonstrated that the scalar charge of neutron stars, emerging in the context of the same theory, is extremely small. We would like to add to this that, according to our analysis, the more stable configurations tend to correspond to black holes with small scalar charge. Perhaps, future observations of gravitational waves from black-hole or neutron-star processes could lead to clear signatures (or impose constraints) on the existence of GB compact objects, provided that these objects have a small mass and/or a large scalar charge. Finally, the measurement of the characteristic frequencies of the quasinormal modes (especially the polar sector) will also help to distinguish these solutions from their GR analogs [36].

ACKNOWLEDGMENTS

G. A. would like to thank Onassis Foundation for the financial support provided through its scholarship program.

Note added.—Recently, two additional works, that studied black-hole solutions with scalar hair in the context of the Einstein-scalar-Gauss-Bonnet theory, appeared [38,39].

APPENDIX A: SET OF DIFFERENTIAL EQUATIONS

Here, we display the explicit expressions of the coefficients P, Q, and S that appear in the system of differential equations (15) and (16), the solution of which determines the metric function A and the scalar field ϕ. They are

$$
\begin{aligned}
P = &+e^{4B}(32A'\dot{f} - 48rA'^2\dot{f} - 8r^2\phi' - 4r^3A'\phi' - 64r\phi'^2\dot{f}) + e^{3B}(-64A'\dot{f} + 96rA'^2\dot{f} \\
&+ 48r^2A'^3\dot{f} + 8r^2\phi' - 4r^3A'\phi' - 4r^4A'^2\phi' + 128A'^2\phi'\dot{f}^2 + 96rA'^3\phi'\dot{f}^2 + 64r\phi'^2\dot{f} \\
&+ 24r^2A'\phi'^2\dot{f} - 20r^3A'^2\phi'^2\dot{f} - 2r^4\phi'^3 + 96rA'\phi'^3\dot{f}^2 - 16r^3\phi'^4\dot{f} + 32r^2\phi'^3\ddot{f} \\
&+ r^5A'\phi'^3 + 16r^3A'\phi'^3\ddot{f}) + 16e^{2B}(8A'\dot{f} - 12rA'^2\dot{f} - 20r^2A'^3\dot{f} - 64A'^2\phi'\dot{f}^2 \\
&- 112rA'^3\phi'\dot{f}^2 - 14r^2A'\phi'^2\dot{f} + 19r^3A'^2\phi'^2\dot{f} - 96A'^3\phi'^2\dot{f}^3 - 32rA'\phi'^3\dot{f}^2 \\
&+ 36r^2A'^2\phi'^3\dot{f}^2 + 8r^3\phi'^4\dot{f} - 4r^4A'\phi'^4\dot{f} - 8r^2\phi'^3\ddot{f} + 4r^3A'\phi'^3\ddot{f} - 32r^2A'\phi'^4\dot{f}\ddot{f}) \\
&+ 16e^{B}(8A'^2\phi'\dot{f}^2 + 38rA'^3\phi'\dot{f}^2 + 64A'^3\phi'^2\dot{f}^3 + 18rA'\phi'^3\dot{f}^2 - 17r^2A'^2\phi'^3\dot{f}^2) \\
&- 1152A'^3\phi'^2\dot{f}^3,
\end{aligned}
\tag{A1}
$$

$$
\begin{aligned}
Q = &+32e^{5B}r - e^{4B}(64r + 24r^2A' + 160\phi'\dot{f} + 48rA'\phi'\dot{f} + 4r^3\phi'^2 + 128r\phi'^2\ddot{f}) \\
&+ e^{3B}(32r + 24r^2A' - 8r^3A'^2 + 320\phi'\dot{f} + 224rA'\phi'\dot{f} - 32r^2A'^2\phi'\dot{f} - 12r^3\phi'^2 \\
&+6r^4A'\phi'^2 + 256A'\phi'^2\dot{f}^2 - 32rA'^2\phi'^2\dot{f}^2 - 24r^2\phi'^3\dot{f} + 12r^3A'\phi'^3\dot{f} - 32r\phi'^4\dot{f}^2 \\
&-r^5\phi'^4 + 256r\phi'^2\ddot{f} + 128r^2A'\phi'^2\ddot{f} + 640\phi'^3\dot{f}\ddot{f} + 256rA'\phi'^3\dot{f}\ddot{f} - 16r^3\phi'^4\ddot{f}) \\
&+ e^{2B}(128r^2A'^2\phi'\dot{f} - 160\phi'\dot{f} - 176rA'\phi'\dot{f} - 640A'\phi'^2\dot{f}^2 + 320rA'^2\phi'^2\dot{f}^2 \\
&+152r^2\phi'^3\dot{f} - 52r^3A'\phi'^3\dot{f} + 128A'^2\phi'^3\dot{f}^3 + 256\phi'^4r\dot{f}^2 - 80r^2A'\phi'^4\dot{f}^2 + 4r^4\phi'^5\dot{f} \\
&-128r\phi'^2\ddot{f} - 128r^2A'\phi'^2\ddot{f} - 1280\phi'^3\dot{f}\ddot{f} - 1280rA'\phi'^3\dot{f}\ddot{f} + 16r^3\phi'^4\ddot{f} \\
&-1280A'\phi'^4\dot{f}^2\ddot{f} + 64r^2\phi'^5\dot{f}\ddot{f}) + e^{B}(384A'\phi'^2\dot{f}^2 - 672rA'^2\phi'^2\dot{f}^2 - 768A'^2\phi'^3\dot{f}^3 \\
&-480r\phi'^4\dot{f}^2 + 144r^2A'\phi'^4\dot{f}^2 + 640\phi'^3\dot{f}\ddot{f} + 1024rA'\phi'^3\dot{f}\ddot{f} + 3584A'\phi'^4\dot{f}^2\ddot{f} \\
&-64r^2\phi'^5\dot{f}\ddot{f}) + 1152A'^2\phi'^3\dot{f}^3 - 2304A'\phi'^4\dot{f}^2\ddot{f},
\end{aligned}
$$

$$
\begin{aligned}
S = &+128r\dot{f}e^{4B} + 8e^{3B}(r^4\phi' - 32r\dot{f} - 16r^2A'\dot{f} - 80\phi'\dot{f}^2 32rA'\phi'\dot{f}^2 + 4r^3\phi'^2\dot{f}) \\
&+ 32e^{2B}(4r\dot{f} + 4r^2A'\dot{f} + 40\phi'\dot{f}^2 + 40rA'\phi'\dot{f}^2 - 3r^3\phi'^2\dot{f} + 40A'\phi'^2\dot{f}^3 - 4r^2\phi'^3\dot{f}^2) \\
&+ 8e^{B}(32r^2\phi'^3\dot{f}^2 - 80\phi'\dot{f}^2 - 128rA'\phi'\dot{f}^2 - 448A'\phi'^2\dot{f}^3) + 2304A'\phi'^2\dot{f}^3.
\end{aligned}
\tag{A2}
$$

APPENDIX B: SCALAR QUANTITIES

By employing the metric components of the line element (7), one may compute the following scalar-invariant gravitational quantities:

$$
R = +\frac{e^{-B}}{2r^2}(4e^B - 4 - r^2A'^2 + 4rB' - 4rA' + r^2A'B' - 2r^2A''),
\tag{B1}
$$

$$
R_{\mu\nu}R^{\mu\nu} = +\frac{e^{-2B}}{16r^4}[8(2 - 2e^B + rA' - rB')^2 + r^2(rA'^2 - 4B' - rA'B' + 2rA'')^2 + r^2(rA'^2 + A'(4 - rB') + 2rA'')^2],
\tag{B2}
$$

$$
R_{\mu\nu\rho\sigma}R^{\mu\nu\rho\sigma} = +\frac{e^{-2B}}{4r^4}[r^4A'^4 - 2r^4A'^3B' - 4r^4A'B'A'' + r^2A'^2(8 + r^2B'^2 + 4r^2A'') + 16(e^B - 1)^2 + 8r^2B'^2 + 4r^4A''^2],
\tag{B3}
$$

$$
R^2_{\rm GB} = +\frac{2e^{-2B}}{r^2}[(e^B - 3)A'B' - (e^B - 1)A'^2 - 2(e^B - 1)A''].
\tag{B4}
$$

[1] K. S. Stelle, Phys. Rev. D **16**, 953 (1977).
[2] T. P. Sotiriou, Lect. Notes Phys. **892**, 3 (2015); E. Berti *et al.*, Classical Quantum Gravity **32**, 243001 (2015).
[3] J. D. Bekenstein, Phys. Rev. Lett. **28**, 452 (1972); C. Teitelboim, Lett. Nuovo Cimento **3**, 397 (1972).
[4] M. S. Volkov and D. V. Galtsov, JETP Lett. **50**, 346 (1989); P. Bizon, Phys. Rev. Lett. **64**, 2844 (1990); B. R. Greene, S. D. Mathur, and C. M. O'Neill, Phys. Rev. D **47**, 2242 (1993); K. I. Maeda, T. Tachizawa, T. Torii, and T. Maki, Phys. Rev. Lett. **72**, 450 (1994).
[5] H. Luckock and I. Moss, Phys. Lett. B **176**, 341 (1986); S. Droz, M. Heusler, and N. Straumann, Phys. Lett. B **268**, 371 (1991).
[6] J. D. Bekenstein, Ann. Phys. (N.Y.) **82**, 535 (1974); Ann. Phys. (N.Y.) **91**, 75 (1975).
[7] J. D. Bekenstein, Phys. Rev. D **51**, R6608 (1995).
[8] T. P. Sotiriou and V. Faraoni, Phys. Rev. Lett. **108**, 081103 (2012).
[9] L. Hui and A. Nicolis, Phys. Rev. Lett. **110**, 241104 (2013).
[10] P. Kanti, N. E. Mavromatos, J. Rizos, K. Tamvakis, and E. Winstanley, Phys. Rev. D **54**, 5049 (1996); Phys. Rev. D **57**, 6255 (1998).
[11] G. W. Gibbons and K. i. Maeda, Nucl. Phys. **B298**, 741 (1988).
[12] C. G. Callan, Jr., R. C. Myers, and M. J. Perry, Nucl. Phys. **B311**, 673 (1989).
[13] B. A. Campbell, M. J. Duncan, N. Kaloper, and K. A. Olive, Phys. Lett. B **251**, 34 (1990); B. A. Campbell, N. Kaloper, and K. A. Olive, Phys. Lett. B **263**, 364 (1991).
[14] S. Mignemi and N. R. Stewart, Phys. Rev. D **47**, 5259 (1993).
[15] P. Kanti and K. Tamvakis, Phys. Rev. D **52**, 3506 (1995).
[16] T. Torii, H. Yajima, and K. i. Maeda, Phys. Rev. D **55**, 739 (1997).
[17] P. Kanti and K. Tamvakis, Phys. Lett. B **392**, 30 (1997).
[18] Z. K. Guo, N. Ohta, and T. Torii, Prog. Theor. Phys. **120**, 581 (2008); N. Ohta and T. Torii, Prog. Theor. Phys. **122**, 1477 (2009); K. i. Maeda, N. Ohta, and Y. Sasagawa, Phys. Rev. D **80**, 104032 (2009); N. Ohta and T. Torii, Prog. Theor. Phys. **124**, 207 (2010).
[19] B. Kleihaus, J. Kunz, and E. Radu, Phys. Rev. Lett. **106**, 151104 (2011); B. Kleihaus, J. Kunz, S. Mojica, and E. Radu, Phys. Rev. D **93**, 044047 (2016).
[20] P. Pani, C. F. B. Macedo, L. C. B. Crispino, and V. Cardoso, Phys. Rev. D **84**, 087501 (2011); P. Pani, E. Berti, V. Cardoso, and J. Read, Phys. Rev. D **84**, 104035 (2011).
[21] C. A. R. Herdeiro and E. Radu, Phys. Rev. Lett. **112**, 221101 (2014).
[22] D. Ayzenberg and N. Yunes, Phys. Rev. D **90**, 044066 (2014); **91**, 069905(E) (2015).
[23] C. Charmousis, Lect. Notes Phys. **769**, 299 (2009).
[24] C. A. R. Herdeiro and E. Radu, Int. J. Mod. Phys. D **24**, 1542014 (2015).
[25] J. L. Blazquez-Salcedo *et al.*, IAU Symp. **12**, 265 (2016).
[26] T. P. Sotiriou and S. Y. Zhou, Phys. Rev. Lett. **112**, 251102 (2014).
[27] E. Babichev and C. Charmousis, J. High Energy Phys. 08 (2014) 106.
[28] T. P. Sotiriou and S. Y. Zhou, Phys. Rev. D **90**, 124063 (2014); R. Benkel, T. P. Sotiriou, and H. Witek, Classical Quantum Gravity **34**, 064001 (2017); Phys. Rev. D **94**, 121503 (2016).
[29] R. R. Metsaev and A. A. Tseytlin, Nucl. Phys. **B293**, 385 (1987).
[30] G. W. Horndeski, Int. J. Theor. Phys. **10**, 363 (1974).
[31] G. Antoniou, A. Bakopoulos, and P. Kanti, Phys. Rev. Lett. (to be published).
[32] G. W. Gibbons and S. W. Hawking, Phys. Rev. D **15**, 2752 (1977).
[33] J. W. York, Jr., Phys. Rev. D **31**, 775 (1985).
[34] G. W. Gibbons and R. E. Kallosh, Phys. Rev. D **51**, 2839 (1995).
[35] S. Bhattacharya and S. Chakraborty, Phys. Rev. D **95**, 044037 (2017); I. Banerjee, S. Chakraborty, and S. SenGupta, Phys. Rev. D **96**, 084035 (2017).
[36] J. L. Blazquez-Salcedo, C. F. B. Macedo, V. Cardoso, V. Ferrari, L. Gualtieri, F. S. Khoo, J. Kunz, and P. Pani, Phys. Rev. D **94**, 104024 (2016).
[37] K. Yagi, L. C. Stein, N. Yunes, and T. Tanaka, Phys. Rev. D **85**, 064022 (2012); **93**, 029902(E) (2016).
[38] D. D. Doneva and S. S. Yazadjiev, arXiv:1711.01187.
[39] H. O. Silva, J. Sakstein, L. Gualtieri, T. P. Sotiriou, and E. Berti, arXiv:1711.02080.